

# Thermo-economic analysis and multi-criteria optimization of an integrated biomass-to-energy power plant

O.J. Ogorure<sup>\*</sup>, F. Heberle, D. Brüggemann

Chair of Technical Thermodynamics and Transport Processes (LTTT), Center for Energy Technology (ZET), University of Bayreuth, Universitätsstrasse 30, 95440, Bayreuth, Germany

## ARTICLE INFO

### Keywords:

Biomass  
Proton exchange membrane electrolyzer  
Organic rankine cycle  
Solid oxide fuel cell  
Multi-criteria optimization

## ABSTRACT

A biomass-driven integrated system comprising anaerobic digestion, gasification, proton exchange membrane electrolyzer (PEME), Sabatier reactor, solid oxide fuel cell (SOFC), a gas turbine, steam turbine and organic Rankine cycle (ORC) was proposed in this study. Biomass feedstocks in form of animal waste served as input in the digester and converted to biogas, and crop residue was converted to syngas in the gasifier. Upgraded syngas and methane from the bio-conversion process was fed to a SOFC-GT topping cycle, with heat recovery bottoming cycles of steam turbine and organic Rankine cycles. The proposed system was assessed from energy, exergy and economic viewpoints in Engineering Equation Solver (EES) software. Parametric analysis was performed to ascertain the effect of design parameters on the plant's performance. Lastly, a multi-criteria optimization was performed using multi-objective genetic algorithm (MOGA) in MATLAB to maximize exergy efficiency and minimize leveled cost of electricity, as well as selection of best ORC working fluid from six preselected candidates (MM, MDM, cyclopentane, cyclohexane, R1233zd(E), and R600a). According to the results, at optimum point the plant can attain energy and exergy efficiencies of 54.81 % and 44.87 %, respectively. The total power output is 9.05 MW, with leveled cost of electricity of 111.8 \$/MWh. Hydrogen of 0.0023 kg/s with PEME efficiency of 73.73 % was obtained and further used in upgrading the syngas from LHV of 4.20–37.78 MJ/kg.

## 1. Introduction

Attaining the feat of sustainable energy is still a major challenge, despite the availability of renewable energy resources in most countries. This is due to the underutilization of renewable resources coupled with global demand for fossil fuels [1]. Sustainable energy development is intended to balance social, environmental and economic considerations of energy conversion systems [2]. In developing countries, such as Nigeria, a country in Sub-Saharan Africa, well-endowed with renewable energy resources, the daunting challenge of meeting energy demands for power generation still persists. Nigeria's current power demand stands at 8.25 GW for a population of 207 million people [3]. With a target of 45 GW generating capacity by 2030, the nation requires an integrated power mix of renewable resources rather than a fossil fuel-based power sector [4]. There is room for the development and evaluation of sustainable solutions that utilize one or more environmentally friendly input such as biomass [5].

Biomass in the form of agrarian waste is regarded as one of such viable renewable resources for bioenergy as it is sustainable and does

not interfere with the food production. This can be in forms of animal waste and crop residue. Despite their varying elemental composition, agrarian waste are potential sources of environmentally friendly fuel gas, obtained through thermochemical or biochemical decomposition [6]. Anaerobic digestion of animal waste, which involves the biochemical decomposition of the waste by microorganisms, results in the production of biogas. Biogas, with compositions of 45–65 % CH<sub>4</sub> and 55–35 % CO<sub>2</sub>, respectively, can be used directly as fuel in gas powered plants, or in fuel cells or converted to chemicals for industrial processes ([7,8]). The thermochemical conversion of biomass includes gasification, combustion and pyrolysis. Gasification is the partial oxidation of the waste, performed at high temperatures of 500 °C–1600 °C, to produce syngas [9]. Syngas consists of CH<sub>4</sub>, CO<sub>2</sub>, H<sub>2</sub>, N<sub>2</sub>, water vapour and other contaminants, depending on the type of biomass. Furthermore, the energy density of syngas is low compared to natural gas, hence the need for it to be upgraded to synthetic natural gas [10]. Due to the complexities from the gasification to cooling processes, heat losses can be minimized through steam generation and converted to useful energy forms such as process heat and electricity. Hybrid digestion-gasification conversion of

<sup>\*</sup> Corresponding author.

E-mail address: [oreva.ogorure@uni-bayreuth.de](mailto:oreva.ogorure@uni-bayreuth.de) (O.J. Ogorure).

biomass has been investigated in previous studies to achieve high yield and enhanced biofuels. He [11] analyzed a biomass-to-syngas and bio-alcohol production process from thermodynamic standpoint. An improved energy efficiency, reduced CO<sub>2</sub> emission and low production cost was obtained for the plant analysis. A study of waste heat conversion for syngas upgrade was performed by Ogorure et al. [12]. They analyzed a hybrid biomass conversion system with integrated ORC-PEME with different ORC working fluids. The maximum energy efficiency of 19.23 % and net power of 0.28 MW was reported with ORC configuration with regenerator using R1233zd(E) working fluid. Low heating value of 50 MJ/kg was obtained for the upgraded syngas.

Multigeneration systems can be a significant potential option to meet local needs by optimum utilization of local resources [13]. These plants allow the integration of several technologies such as combined, multi-stage, hybrid and cascaded energy systems. The technique can be employed in plants with the potential for high thermal energy generation, such as thermo-chemical conversion of biomass or gasification [14]. Safari and Dincer [1] evaluated a biogas multigeneration plant with biogas produced from anaerobic digestion of sewage sludge and with useful outputs of power, heat, freshwater, and hydrogen from the integration of the PEME. With net power of 2.17 MW from a gas turbine (GT) and ORC units, the total energy and exergy efficiencies of the plant were obtained as 63.6 % and 40 %, respectively. Ogorure et al. [15] considered a waste-to-energy multigeneration plant with a gasifier and anaerobic digester. They demonstrated the successful integration of several thermodynamic cycles from the utilization of bio-syngas. Net power of 5.226 MW with energy and exergy efficiencies of 63.62 % and 58.46 % was obtained for the configuration. However, they did not consider the thermodynamic analysis of the biomass to bio-syngas process. Tukenmez et al. [16] analyzed a multigeneration plant for ammonia and hydrogen production with syngas from biomass and solar sources. A net power of 20 MW, with plant energy and exergy efficiencies of 58.76 % and 55.64 % respectively, and hydrogen generation rate of 0.0855 kg/s were obtained. Taheri et al. [17] performed a multi-objective optimization of a biomass-based multigeneration plant aimed at producing power, cooling, natural gas, and hydrogen. The plant consisted of a gasifier, combined gas and steam turbine, cascaded Rankine cycles, absorption refrigeration unit, PEME and a liquid natural gas subsystem. An exergy efficiency of 39.023 % and total product cost rate of 1107 \$/h was obtained from the optimization results through genetic algorithm. Karimi et al. [18] investigated a biomass-based heat and power plant with rice straw as feedstock in a gasifier-SOFC-GT-ORC plant. They reported the SOFC current density had the largest impact on the systems efficiency and cost rate. Through multi-objective optimization, an optimum exergy efficiency of 35.1 %, cost rate of 10.2 \$/h, and largest irreversibility in the gasifier. The integration of a SOFC-GT topping cycle with a biogas reforming cycle was carried out by Solaymani et al. [19]. Thermal energy exiting the SOFC-GT unit was used for the reforming cycle in the production of hydrogen. A net power, exergy efficiency, and hydrogen flow rate of 2.72 MW, 64.65 % and 0.07453 kg/s were obtained from the thermodynamic analysis of the configuration. A large amount of exergy destruction of 26 % of total exergy destruction rate was observed in the afterburner. Holagh et al. [20] proposed a combined system with SOFC, gas turbines, biomass burner, ORC, refrigeration cycle, desalination unit, and PEME. An exergo-economic and environmental analysis of the system revealed a net power of 4.4 MW, refrigeration capacity of 0.16 MW, with desalinated water of 0.96 kg/s. A hydrogen production rate of 0.00155 kg/s, costs per unit exergy 11.28 \$/GJ, a total cost rate of product of 223 \$/h and an estimated CO<sub>2</sub> emission of 10.79 kmol/MWh were obtained for the configuration. Emadi et al. [21] examined the potential of a dual-loop ORC system in improving the performance of an integrated SOFC-GT topping cycle. They employed artificial neural network and multi-objective optimization approach in investigating 20 combinations of ORC working fluids. R601 and Ethane (for topping and bottom cycle, respectively) indicated best results of 51.3 % overall system exergy

efficiency and net electrical power of 1.04 MW. Also, the levelized cost of electricity (LCOE) for the SOFC-GT-ORC was 33.2 \$/MWh, which was 12.9 % and 73.9 % less than SOFC-GT and SOFC cycles, respectively. Sevinchan et al. [22] developed a biomass based multigeneration system of 1.078 MW net power, 0.198 MW heat capacity and 87.54 kW cooling load. Both energy and exergy efficiencies increased with increasing useful outputs. Highest exergy destruction rate of 65 % was recorded in the combustion chamber, with evaporator of ORC and biomass digester having 9.2 % and 14.3 %.

Malik et al. [23] analyzed a multigeneration system with combined primary energy sources of biomass combustion unit and a geothermal power plant. Both sources were utilized in an ORC, absorption chiller cycle, Linde-Hampson liquefaction cycle, a water heating system and a dryer. The energy and exergy efficiencies of the system were 56.5 % and 20.3 %, respectively, with high exergy destruction recorded in the combustion chamber and boiler. Ahmadi et al. [24] developed a multigeneration plant fueled by biomass combustion for power generation, hydrogen production and cooling purposes. A combination of domestic water heater, ORC, absorption refrigeration and PEME were used in the plant configuration. The results indicated the combustor and ORC evaporator as two main sources of irreversibility and the pinch point temperatures had high effect on the systems performance. Also, the potential for CO<sub>2</sub> emission reduction was high for the configuration when compared to a conventional power generation plant. Bamsile et al. [25] considered a biogas powered trigeneration configuration for electricity, cooling and heating, incorporating the concepts of combined reheat and regeneration in two steam cycles. The performance of the system in terms of energy and exergy improved from 43.96 % to 33.34 %–64.00 % and 34.51 %, respectively, when more than one useful output was produced. An integrated system analyzed based on the first and second laws of thermodynamics was proposed by Anvari et al. [26]. They presented exergo-economic and thermodynamic viability of integrating gas turbine, with HRSG, absorption refrigeration and regenerative ORC for power and heating. Yilmaz et al. [27], enumerated high thermodynamic performance and lower CO<sub>2</sub> emissions as attributes associated with biogas multigeneration systems. According to their results, increase in GT inlet temperature by 400 °C increased the production rate of hydrogen from 0.04 kg/s to about 0.10 kg/s and electricity generation from 7.5 MW to 15 MW, respectively. Al-Rashed and Afrand [28] optimized a combined GT with supercritical CO<sub>2</sub> (S-CO<sub>2</sub>) system driven by biogas generated from anaerobic digestion. Multi-criteria optimization of the system resulted in a total product cost improvement of 24.6 % with inlet cooling of CO<sub>2</sub> when compared to the configuration without inlet cooling. Balafkandeh et al. [29] performed a multi-objective optimization on a biomass fueled multi-generation plant integrated with gas turbine, supercritical CO<sub>2</sub> unit and absorption refrigeration system. A comparison of the system performance under biomass to syngas from gasification and biomass to biogas from digestion indicated improved results of 47.8 % exergy efficiency and unit product cost of 5.436 \$/GJ with the biogas fuel. Pure ORC working fluids and zeotropic mixtures were investigated under three heat sources of syngas cooling unit, air separation unit and carbon capture unit by Georgousopoulos et al. [30]. They presented the thermodynamic and techno-economic assessment of a waste heat recovery ORC in a biomass integrated gasification combined cycle under several scenarios of ORC working fluids. Highest plant efficiency improvement of 2.86 % was obtained in the syngas cooling scenario, with best economic performance of 35.42–35.67 €/MWh LCOE and 5.7–5.8 years of payback period. Also, zeotropic mixtures had relatively small economic advantage over pure fluids.

From the review of literature, the application of multigeneration plants have been studied by researchers with results indicating a promising option for biomass-fueled heat and power systems. However, a hybrid biomass conversion system combining anaerobic digestion, gasification and methanation integrated with power powerplant is yet to be investigated under thermo-economic principles. Also, the

optimization of the plant, with ORC fluid selection is rarely noticed in the review of literature.

The main objectives of this study are listed as follows:

- To develop an integrated biomass conversion system based on the gasification and anaerobic digestion (AD) of agrarian waste for power, and hydrogen (utilized during syngas upgrade) in a Nigerian locality.
- To analyze the overall system from a thermodynamic and economic points of view.
- To investigate the effect of some operating parameters, as well as the choice of ORC working fluid on the system outputs.
- To perform multi-objective optimization of the power section for the best system performance.

The locality adopted for this study is south-east of Rivers state in southern Nigeria with a population of 1.78 million. The estimated power consumption of this region stands at 240 GWh and is barely available. Enormous amount of biowaste is generated in this region and it is expected to adequately support energy recovery through biowaste conversion. Realistic values for each locality's annual biowaste generation are required to estimate the required biowaste flow input to the biomass section in the plant. However, due to a lack of census data, accurate reported data may not always be available, necessitating an estimation based on previous reported data. In this paper, the approach proposed by Ogorure et al. [15] to estimate the quantity of biowaste produced and its conversion was adopted. They developed a model to predict the amount of waste from previous farm data of crop and animal waste for an agro-facility in the locality of interest.

## 2. Methodology

### 2.1. System description

The schematic diagram of the proposed plant is presented in Fig. 1, with the bio-conversion unit (BCU) integrated with an ORC and PEME. Anaerobic digestion and gasification are employed in the conversion of biomass feedstock into gaseous fuel. The biomass feedstock comprises of animal waste which is fed to the digester due to high humidity content, and crop waste which is converted through gasification. Syngas from the

gasification process is cooled to low temperatures in a syngas heat exchanger (HXS) and fed to a methanation unit (MTH). Steam recovered from the syngas cooling is utilized in ORC I for power generation. A PEME is employed in producing hydrogen for the methanation process with upgraded synthetic natural gas as end product. Cleaned biogas from the digestion process is fed to a combined SOFC-GT topping cycle to produce power. The SOFC through electrolysis converts the mixture of air and gaseous fuel (stream 29 and stream 33) into power, part of which is consumed by the PEME. Excess fuel from the SOFC process, along with additional fuel from the methanation process is combusted in a combustion chamber (CC). The high temperature gas from the combustion process drives the GT generating power by expansion. The gas stream (36) at high temperature passes through the fuel and air pre-heaters (HX1 and HX2) raising the temperature of fuel and air entering the SOFC. Flue gas exiting the topping cycle (stream 38) is utilized for further power generation in a steam turbine (ST) plant. Due to the high thermal energy of the flue gas from the heat recovery steam generator (HRSG) of the ST plant, it is fed to an organic Rankine cycle (ORC II) unit and further converted to power.

### 2.2. Thermodynamic assessment

Analysis and assessment of the biomass fueled configuration is evaluated on both energy and exergy performances of the plant based of the first and second laws of thermodynamics. Computation was made in Engineering Equation Solver (EES) for the evaluation of the systems performance as well as of the exergy destroyed. General assumptions made for the plant analysis include:

- Steady flow and steady state operating conditions throughout the system.
- Negligible changes in potential and kinetic energy and exergy in the plant streams.
- Ambient temperature and pressure are 298.15 K and 101.325 kPa, respectively.
- Air composition of 79 % nitrogen and 21 % oxygen.
- ORC maximum operating pressure of  $0.9 P_{cr}$ .
- Ideal gas condition is assumed for all gas streams in the plant.
- Downdraft gasifier is assumed for gasification unit.

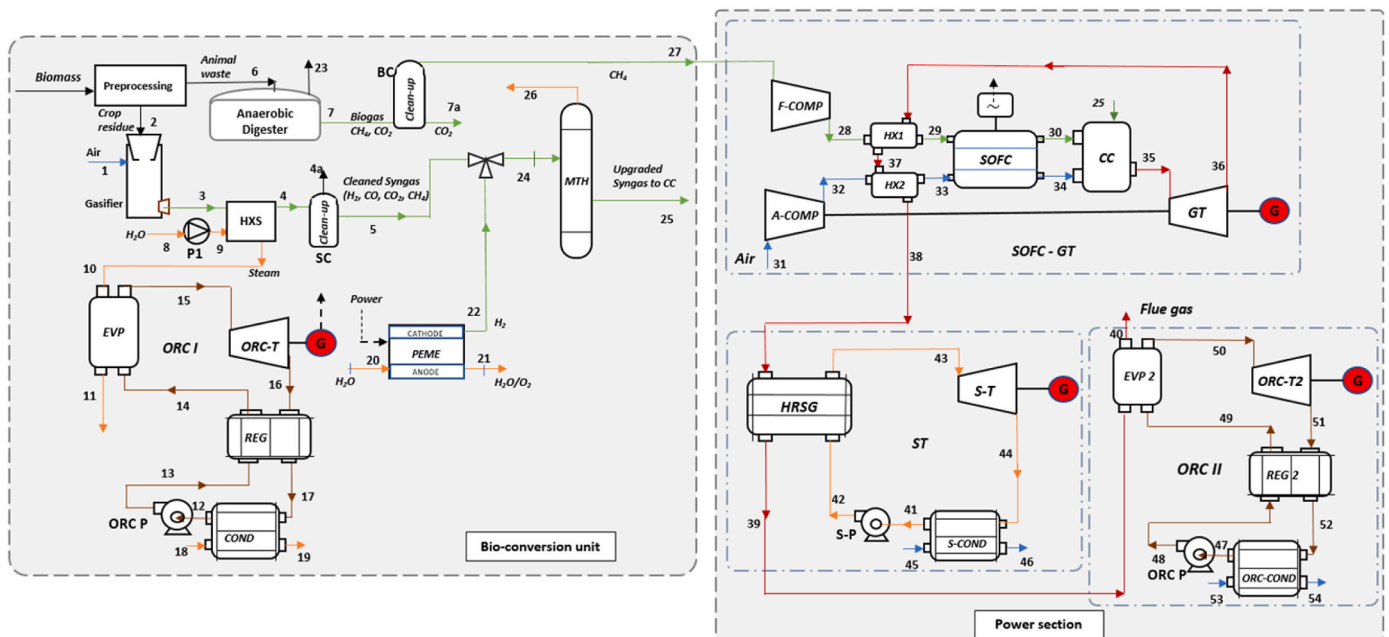


Fig. 1. Schematic of the proposed bio-fueled power plant with biomass conversion and power sections.

- Negligible heat losses in the SOFC-GT system as well as the gasification and methanation process.

The control volume approach is adopted in modeling plant components where mass, energy, and exergy balance equations are applied. Under steady condition, mass, energy and exergy balance relations are given as:

$$\text{Mass balance : } \sum \dot{m}_{in} = \sum \dot{m}_{out} \quad (1)$$

$$\text{Energy balance : } \sum \dot{m}_{in}h_{in} + \dot{Q} = \sum \dot{m}_{out}h_{out} + \dot{W} \quad (2)$$

$$\text{Exergy balance : } \sum \dot{E}x_{in,k} = \sum \dot{E}x_{out,k} + \dot{E}x_{D,k} \quad (3)$$

where  $\dot{m}$  is the mass flow rate,  $h$  is the specific enthalpy of the stream,  $\dot{Q}$  and  $\dot{W}$  are the heat and power transfer rates, respectively. Neglecting elevation and velocity variation, specific exergy is expressed in terms of chemical and physical exergy as

$$e = e^{ch} + e^{ph} \quad (4)$$

where  $e^{ch}$  and  $e^{ph}$  of the  $i$ -th species are obtained by

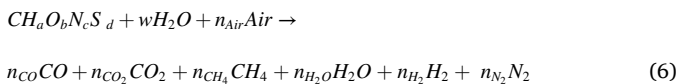
$$e_i^{ch} = \sum_{i=1}^n y_i e_{0,i}^{ch} + RT_0 \sum_{i=1}^n y_i \ln(y_i) \quad (5)$$

$e_{0,i}^{ch}$  and  $y_i$  are standard chemical exergy and mole fraction of the  $i$ -th species.

Based on the above governing equations, energy and exergy balance equations of each component of the integrated plant are presented in [Appendix A](#).

### 2.3. Gasifier

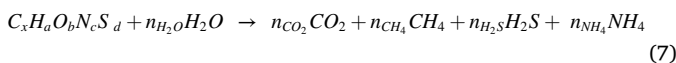
The biomass downdraft gasifier is operated at high temperature to yield high grade synthesis gas. The global gasification reaction in the gasifier with air as gasifying agent is given as:



where  $CH_aO_bN_cS_d$ ,  $w$ , and  $n_i$  are the crop waste chemical formula in terms of carbon, moisture content and amount in mole of the  $i$ -th species specified in the equation. Evaluation of equation (6) was according to suggested methods by Athari et al. [31].

### 2.4. Digester

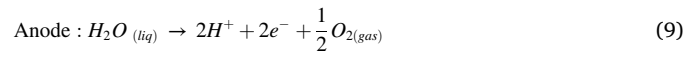
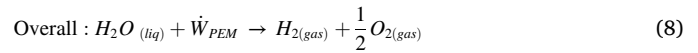
The chemical reaction of the anaerobic digestion process is



where  $C_xH_aO_bN_cS_d$  represents the animal waste formula.  $x, a, b, c, d$  are known number of atoms for C, H, O, N, and S, defined from the ultimate analysis in [Table 3](#). The modified Buswell method according to Allesina et al. [32] is applied in estimating the biogas composition using the ultimate analysis.

### 2.5. PEME

The reactions inside an electrolyzer are akin to that of a fuel cell however in a reverse direction. The overall, anode and cathode reactions regarding the production of hydrogen in the PEME are expressed as [20].



Also, the molar rate balance of hydrogen, oxygen and water reacted by each cell of the electrolyzer can be evaluated as

$$\dot{n}_{H_2,22} = \frac{N_E j_E A_E}{2F} \quad (11)$$

$$\dot{n}_{O_2,21} = \frac{1}{2} \dot{n}_{H_2,22} \quad (12)$$

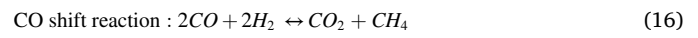
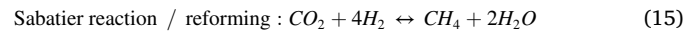
$$\dot{n}_{H_2O,20} = 2\dot{n}_{H_2,22} + \dot{n}_{O_2,21} + \dot{n}_{H_2O,21} \quad (13)$$

$$\dot{n}_{H_2O,20} = 2\dot{n}_{H_2,22} + \dot{n}_{O_2,21} \quad (14)$$

where  $\dot{n}_i$  is the molar conversion rate of the  $i$ -th species in equations (11)–(14),  $N_E, j_E, A_E$ , are the number of cells, current density and active surface area of the PEME. The electrical power, current density, Nernst voltage, voltage and ohmic losses of the electrolyzer are described in [Table 1](#).

### 2.6. Methanation

In the methanation reactor,  $CO_2$  and  $CO$  from the gasification process are converted to SNG through two exothermic reactions:



Gibbs free energy of chemical equilibrium is applied in determining the molar composition of the SNG with reactants of the gasification product and  $CO_2$  from the digestion process. The total Gibbs free energy of the equations is expressed as [33]

$$G = \sum_{i=1}^M n_i \mu_i = \sum_{i=1}^M n_i \mu_i^o + RT \sum n_i \ln \left( \frac{y_i P}{P_0} \right) \quad (17)$$

Under mass balance constraints, Lagrange multipliers  $\lambda_i$  for each species  $i$  are introduced, such that

$$\mu_i + \sum_{j=1}^K \lambda_j n_{ij} = 0 \quad (18)$$

Combining both equations yields

$$\mu_i^o + RT \sum_{j=1}^K \lambda_j n_{ij} = 0 \quad (19)$$

Expressing equation (19) in terms of the unknown species results in a system of linear simultaneous equations, which is solved to obtain an approximation of the minimum free energy to convergence.

### 2.7. SOFC

The SOFC ability to simultaneously utilize carbon monoxide and hydrogen as fuel is an important and characteristic feature. Through the direct internal reforming occurring inside the fuel cell, methane and carbon monoxide result as a fuel mixture. The key chemical reactions in the SOFC are:

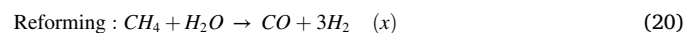
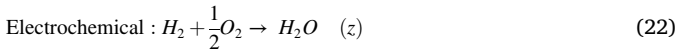


**Table 1**  
Electrochemical equations for PEME and SOFC [20,34].

PEME	SOFC
<b>Power</b>	
$\dot{W}_{PEME} = N_{EjE} A_E V_E$	$\dot{W}_{SOFC} = N_{FCjFC} A_{FC} V_{FC}$
	$\rho = \dot{W}_{SOFC} / A_{FC}$
<b>Current and current density</b>	
$I_E = j_E A_E$	$I_{FC} = j_{FC} A_{FC}$
<b>Cell voltage</b>	
$V_{PEME} = E_{Nerst,E} + V_{Act,a} + V_{Act,c} + V_{Ohm}$	$V_{SOFC} = E_{Nerst,FC} - (V_{Act,a} + V_{Act,c} + V_{Ohm})$
<b>Nernst voltage</b>	
$E_{Nerst,E} = 1.229 - 8.5 \times 10^{-4} (T_E - T_0)$	$E_{Nerst,FC} = -\frac{\Delta g^0}{2F} + \frac{\bar{R}T_{FC}}{2F} \ln \left( \frac{a_{H_2,30} a_{O_2,34}^2}{a_{H_2O,30}} \right)$
	$\Delta g^0 = g_{H_2O}^0 - g_{H_2}^0 - \frac{1}{2} g_{O_2}^0$
	$g^0 = h - T_{FC} s^0$
	$a_{H_2,30} = \frac{y_{H_2,30} P_{30}}{P_0}; a_{O_2,34} = \frac{y_{O_2,34} P_{34}}{P_0}$
	$a_{H_2O,30} = \frac{y_{H_2O,30} P_{30}}{P_0}$
<b>Activation loss</b>	
$V_{Act,a} = \frac{\bar{R}T}{F} \sinh^{-1} \left( \frac{j_E}{2j_{0,a}} \right); j_{0,a} = j_{0,a}^{ref} \exp \left( \frac{-E_{Act,a}}{\bar{R}T_E} \right)$	$V_{Act,a} = \frac{\bar{R}T_{FC}}{F} \sinh^{-1} \left( \frac{j_{FC}}{2j_{0,a}} \right)$
$V_{Act,c} = \frac{\bar{R}T_E}{F} \sinh^{-1} \left( \frac{j_E}{2j_{0,c}} \right); j_{0,c} = j_{0,c}^{ref} \exp \left( \frac{-E_{Act,c}}{\bar{R}} \right)$	$V_{Act,c} = \frac{\bar{R}T_{FC}}{F} \sinh^{-1} \left( \frac{j_{FC}}{2j_{0,c}} \right)$
<b>Ohmic loss</b>	
$V_{Ohm} = j_E R_E$	$V_{Ohm} = j_{FC} (R_C + \sum \rho_i L_i)$
$R_E = \int_0^1 \frac{dx}{\sigma[\lambda(x)]}; \lambda(x) = \frac{\lambda_a - \lambda_c}{L} x + \lambda_c$	$\rho_a = \left( 9.5 \times \frac{10^7}{T_{FC}} \exp \left( -\frac{1150}{T_{FC}} \right) \right)^{-1}$
$\sigma[\lambda(x)] = 0.5139 - 0.326 \exp \left[ 1268 \left( \frac{1}{303} - \frac{1}{T_E} \right) \right]$	$\rho_c = \left( 4.2 \times \frac{10^7}{T_{FC}} \exp \left( -\frac{12000}{T_{FC}} \right) \right)^{-1}$
	$\rho_{el} = \left( 3.34 \times 10^4 \exp \left( -\frac{10300}{T_{FC}} \right) \right)^{-1}$
	$\rho_{int} = \left( 9.3 \times \frac{10^6}{T_{FC}} \exp \left( -\frac{1150}{T_{FC}} \right) \right)^{-1}$
<b>Activation concentration loss</b>	
$V_{conc} = \frac{\bar{R}T_E}{\alpha 2F} \left( 1 - \frac{j_E}{j_l} \right)$	$V_{conc,a} = \frac{\bar{R}T_{FC}}{2F} \left( \ln \left( 1 + \frac{P_{H_2} j_{FC}}{P_{H_2O} j_{a,s}} \right) - \ln \left( 1 - \frac{j_{FC}}{j_{a,s}} \right) \right)$
	$V_{conc,c} = -\left( \frac{\bar{R}T_{FC}}{4F} \ln \left( 1 - \frac{j_{FC}}{j_{c,s}} \right) \right)$
	$j_{a,s} = 2.F.P_{H_2}.D_{a,eff} / \bar{R}T_{FC}.L_a$
	$j_{c,s} = 4.F.P_{O_2}.D_{c,eff} / \left( \left( \frac{P_{33} - P_{O_2,33}}{P_{33}} \right) \bar{R}T_{FC}.L_c \right)$



where  $x$ ,  $y$ ,  $z$ , are the molar conversion rates of the gases in the reforming, shift and electrochemical reactions, respectively. Using molar balance of the reacting gas species with established air and fuel utilization factors,  $UF_{air}$  and  $UF_f$ , respectively. The mass balance, between the inlet and exit of the SOFC can be evaluated with respect to the molar conversion rates  $x_{29}$ ,  $y_{29}$  and  $z_{29}$  from the shift, electrochemical and reforming equations (23)–(32) as:

$$\dot{n}_{CH_4,30} = \dot{n}_{CH_4,29} - x_{29} \quad (23)$$

$$\dot{n}_{H_2,30} = \dot{n}_{H_2,29} + 3x_{29} - y_{29} - z_{29} \quad (24)$$

$$\dot{n}_{CO,30} = x_{29} - y_{29} \quad (25)$$

$$\dot{n}_{CO_2,30} = \dot{n}_{CO_2,29} + y_{29} \quad (26)$$

$$\dot{n}_{H_2O,30} = \dot{n}_{H_2O,29} - x_{29} - y_{29} + z_{29} \quad (27)$$

$$K_s = \frac{\dot{n}_{CO_2,30} \times \dot{n}_{H_2,30}}{\dot{n}_{CO,30} \times \dot{n}_{H_2O,30}} \quad (28)$$

$$K_r = \frac{\dot{n}_{CO,30} \times \dot{n}_{H_2,30}^3}{(\dot{n}_{CH_4,30} \times \dot{n}_{H_2O,30}) \left( \frac{P_{29}}{P_{29}} \right)^2} \quad (29)$$

$$z_{29} = UF_{fuel} (\dot{n}_{H_2,29} + 3x_{29} + y_{29}) \quad (30)$$

$$\dot{n}_{O_2,34} = \dot{n}_{O_2,33} - \frac{z_{29}}{2} \quad (31)$$

$$UF_{air} = \frac{z_{29}}{2\dot{n}_{O_2,33}} \quad (32)$$

where  $K_s$  and  $K_r$  are equilibrium constants of the shift and reforming equations. Both parameters were obtained as in Ref. [15].  $UF_{air}$  and  $UF_{fuel}$  are the air and fuel utilization factors, respectively. The SOFC power, current density, Nernst voltage, voltage and ohmic losses are presented in Table 1.

## 2.8. Organic rankine cycle working fluid selection

The optimal utilization of heat sources and achievement of high performance are two important factors in the selection of ORC working fluids. The thermophysical properties of the working fluid as well as the quality of the heat source are also crucial in achieving this goal. However, emphasis is also made on their environmental effects which include toxicity, flammability, ozone depletion potential (ODP) and global warming potential (GWP). Hence, the choice of 6 ORC working fluids spread across three groups, namely, siloxanes (hetamethylsiloxane, MM and octamethyltrisiloxane, MDM), hydrocarbons (cyclopentane and cyclohexane) and refrigerants (R1233zd(E) and R600a) as listed in Table 2 is made in this study. These fluids are selected in order to optimize the performance of the ORC.

The system's performance is evaluated from both thermodynamic and economic standpoints. Performance indices considered include the plant exergy efficiency,  $\eta_{ex}$ , net power,  $\dot{W}_{net}$ , and levelized cost of electricity,  $LCOE$ . These parameters are defined thus:

$$\eta_{th} = \frac{\dot{W}_{net}}{\dot{Q}_{in}} = \frac{\dot{W}_{SOFC-GT} + \dot{W}_{ST} + \dot{W}_{ORCI} + \dot{W}_{ORCII}}{\dot{m}_{waste} LHV_{waste}} \quad (33)$$

$$\eta_{ex} = \frac{\dot{W}_{net}}{\dot{E}x_{in}} = \frac{\dot{W}_{net}}{\dot{E}x_{waste}} \quad (34)$$

The specific chemical exergy of the waste is obtained according to the relationship [36].

$$e_{waste}^{ch} = \beta_{waste} LHV_{waste} \quad (35)$$

$$\beta_{waste} = \frac{1.0414 + 0.0177 \left( \frac{H}{C} \right) - 0.3328 \left( 1 + 0.0537 \left( \frac{H}{C} \right) + 0.0493 \left( \frac{N}{C} \right) \right)}{1 - 1.4021 \left( \frac{H}{C} \right)} \quad (36)$$

$$LHV_{waste} = 4.187(81C + 300H - 26(O - S) - 6(9H + MC)) \quad (37)$$

where  $\beta_{waste}$  is the ratio of chemical exergy to low heating value of waste.

**Table 2**

Thermophysical, safety and environmental properties of selected working fluids (Douvartzides et al. [35]; Emadi et al. [21]).

Parameter	MM	MDM	Cyclopentane	Cyclohexane	R1233zd(E)	R600a
$T_{crit}$ (K)	518.75	564.09	511.72	553.64	439.6	408
Critical pressure (bar)	19.3	14.1	45.7	40.7	35.7	36.3
ODP	n.a.	n.a.	0	0	0.00024	0
GWP	n.a.	n.a.	0	low	7	4
ASHREA safety group	n.a.	n.a.	n.a.	A3	A1	A3

## 2.9. Economic analysis

The leveled cost of electricity is a key economic parameter that portrays the cost effectiveness of the multigeneration plant. This parameter is defined as the ratio of the annualized cost of the system to the effective electricity in kWh produced by the plant and is evaluated as ([37,38]):

$$LCOE = \frac{ACC (\$/yr)}{TEE (kWh)} \quad (38)$$

$$ACC = Z_{TCI} \times CRF \quad (39)$$

$$CRF = \frac{i_r(1 + i_r)^n}{(1 + i_r)^n - 1} \quad (40)$$

where  $ACC$ ,  $TEE$ ,  $Z_{TCI}$ ,  $CRF$ ,  $i_r$ , and  $n$  are the annual capital cost, total effective electricity, total capital investment cost, capital recovery factor, interest rate and operating life of the plant, respectively (see Table 3). To adjust equipment cost from a specific reference year to a chosen year, the following scaling in equation (42) was applied

$$Z_f = \frac{CEPCI_{chosen\ year}}{CEPCI_{ref\ year}} \quad (41)$$

$$Z_{TCI} = Z_f(Z_{TM} + Z_{Aux}) \quad (42)$$

$$Z_{TM} = 1.18 \sum Z_{BM} \quad (43)$$

$$Z_{BM} = Z_p^o F_{BM} \quad (44)$$

$$Z_{Aux} = 0.3 \sum_{k=1}^{n_{eq}} Z_{BM,k}^o \quad (45)$$

$$\log_{10}(Z_p^o) = K_1 + K_2 \log_{10} Q + K_3 (\log_{10} Q)^2 \quad (46)$$

$$f_{BM} = B_1 + B_2 f_{MP} \quad (47)$$

$$\log_{10}(f_p) = C_1 + C_2 \log_{10} P_g + C_3 (\log_{10} P_g)^2 \quad (48)$$

where  $CEPCI$  is the chemical engineering plant cost index, the reference year according to Turton et al. [37] is 2011 and chosen year is 2020.  $Z_{TM}$ ,  $Z_{Aux}$ ,  $Z_p^o$ ,  $Z_{BM}$  and  $Z_{BM,k}^o$  are the total module cost, auxiliary cost, bare module cost and bare module cost of equipment  $k$  without pressure and material correction factors, respectively.  $Q$  and  $P_g$  represents the

component capacity and  $K_1$ ,  $K_2$ ,  $K_3$ ,  $B_1$ ,  $B_2$ ,  $C_1$ ,  $C_2$ ,  $C_3$ ,  $f_M$ ,  $f_P$  are cost price correction factors, listed in Appendix B.

## 2.10. Optimization

The multi-objective genetic algorithm (MOGA) is a modified optimization algorithm designed to manage multiple competing objectives. In contrast to conventional genetic algorithms having a single objective, MOGA applies a number of objective functions to estimate the fitness of a population. The purpose of MOGA is to identify a set of optimum solutions, which satisfactorily finds a balance between the various objectives. This is carried out by generating a set of solutions known as the Pareto front, which covers the entire space of generated solutions. The Pareto front represents the best trade-off between the various objectives. No Pareto front solution can be enhanced in one without affecting the other. In MOGA, population members are assessed using the various objectives, and the best members are chosen based on how well they manage the competing objectives. In order to create a new population, the chosen individuals are then recombined through crossover and mutation operations. Several generations of this process must pass before the Pareto front is obtained [41]. In this study, the functions considered as objectives are the exergy efficiency and LCOE of the power plant. The optimization model is defined as

$$Max\{\eta_{ex}, -LCOE\} \quad (49)$$

The objective function is analyzed under the following constraints of several decision variables in Table 3:

For the combined optimization, each point on the Pareto curve represents an optimal solution. Hence, LINMAP, a decision method meant to balance the relative importance of the objectives was applied. LINMAP method was executed by first obtaining a Euclidean non-dimensional set of values of the objective functions in the Pareto front using equation (48). An ideal point at which both objectives possess the best values is considered, and the positive Euclidean distance of all points to this ideal solution is obtained as in equation (49). The best value is the point with the lowest distance [6]:

$$f_{ij}^* = \frac{f_{ij}}{\sqrt{\sum (f_{ij})^2}} \quad (50)$$

$$d_i = \sqrt{\sum_{j=1}^m (f_{ij} - f_{i,ideal}^*)^2} \quad (51)$$

where  $f_{ij}^*$  is the non-dimensional solution,  $f_{ij}$  is the  $i$  th solution in the Pareto front,  $j$  is the number of objectives,  $d_i$  is the Euclidean distance from the ideal solution.

## 3. Results and discussion

In this section, the results of the thermodynamic and economic modelling of the system performed in Engineering Equation Solver (EES) are presented and discussed.

**Table 3**

Domain of decision variables.

Variable	Range
$r_p$	$5 \leq r_p \leq 10.5 (-)$
$j_{SOFC}$	$5000 \leq j_{SOFC} \leq 10000 (A/m^2)$
$T_{35}$	$1200 \leq T_{35} \leq 1350 (K)$
$P_{43}$	$5500 \leq P_{43} \leq 10000 (kPa)$
$\Delta p_{pSt}$	$10 \leq \Delta p_{pSt} \leq 50 (K)$
$\theta$	$0.10 \leq \theta \leq 0.9 (-)$
$\Delta p_{ORCII}$	$5 \leq \Delta p_{ORCII} \leq 15 (K)$
$\Delta sh_{ORCII}$	$2 \leq \Delta sh_{ORCII} \leq 15 (K)$

### 3.1. Boundary condition (base case)

Table 4 summarizes the plant specifications sourced from literature. The ultimate analysis of animal and crop waste were obtained from Ogorure et al. [15]. The animal waste comprises of waste obtained from cattle, pigs and poultry, while crop waste consists of rice husk, maize

**Table 4**  
Input data [1,15,20,21,27,28,33,34,39].

Ambient temperature	298 K
Ambient pressure	101.325 kPa
Ultimate analysis of animal waste	44.26 % C 5.95 % H 32.69 % O 5.66 % N 1.21 % S
Ultimate analysis of crop waste	46.45 % C 5.40 % H 38.69 % O 0.64 % N 0.03 % S
Gasifier temperature	1023 K
Gasifier pressure	101.325 kPa
Digester temperature	328.2 K
<b>PEME</b>	
Temperature	353 K
Pressure	101.325 kPa
Current density	1000 A/m <sup>2</sup>
Activation area	0.01 m <sup>2</sup>
Amount of water at anode	14
Amount of water at cathode	10
Thickness	100 μm
Activation power at anode	7.6 × 10 <sup>4</sup> J/kmol
Activation power at cathode	1.8 × 10 <sup>4</sup> J/kmol
Pre-exponential indicator at anode	1.7 × 10 <sup>5</sup> A/m <sup>2</sup>
Pre-exponential indicator at cathode	4.6 × 10 <sup>3</sup> A/m <sup>2</sup>
Faraday constant	96486 C/mol
Number of electrons	2 (–)
<b>ORC</b>	
Operating pressure	0.9 P <sub>cr</sub>
Working fluid	MM
Isentropic efficiency of turbine	84 %
Isentropic efficiency of pump	85 %
Pinch point temperature Evap	10 K
Pinch point temperature Cond	5 K
Pinch point temperature Regenerator	4 K
Degree of superheating	10 K
<b>Methanation</b>	
Pressure	1000 kPa
Temperature	500 K
<b>SOFC</b>	
Current density	5500 A/m <sup>2</sup>
Temperature	1023 K
Activation area	0.08 m <sup>2</sup>
Fuel utilization factor	0.85 (–)
Air utilization factor	0.15 (–)
Exchange current density of anode	6500 A/m <sup>2</sup>
Exchange current density of cathode	2500 A/m <sup>2</sup>
Anode thickness	0.05 × 10 <sup>−2</sup> m
Cathode thickness	0.005 × 10 <sup>−2</sup> m
Thickness of electrolyte	0.001 × 10 <sup>−2</sup> m
Thickness of interconnect	0.03 × 10 <sup>−2</sup> m
Effective gaseous diffusivity, anode	0.2 × 10 <sup>−4</sup> m <sup>2</sup> /s
Effective gaseous diffusivity, cathode	0.05 × 10 <sup>−4</sup> m <sup>2</sup> /s
Number of cells	10000
Steam to carbon ratio	2.5 (–)
Inverter efficiency	95 %
<b>GT</b>	
Isentropic efficiency of turbine	85 %
Isentropic efficiency of compressor	85 %
Pressure ratio	10.5 (–)
<b>ST</b>	
Turbine inlet pressure	6000 kPa
<b>Economic</b>	
Plant life	20 years
Interest rate	12%
Annual operation	8000 h
Maintenance factor	1.06 (–)

stover, palm fruit effluent and cassava peel. The gasification temperature was selected based on optimum conditions from the simulation of the gasification of combined crop waste from Ogorure et al. [15]. For faster reaction rates, thermophilic digester temperature is considered for the anaerobic digester [28]. PEME was modeled according to Saeed and Warkozek [34], and Holagh et al. [20]. ORC parameters with operating pressure, evaporator and condenser pinch points were sourced from Emadi et al. [21]. A tubular SOFC model specification is adopted according to Holagh et al. [20]. Turbine efficiency of over 80 % was selected for the plant's turbines in order to maximize the output of the energy source. In matching system temperature and pressure for integration, the choice of subsystems was considered based on the quality of resource available to each subsystem and the temperature requirements of the subsystems. For subsystems with heat exchangers, the pinch point approach was used to determine the temperature of the hot and cold streams.

### 3.2. Model validation

Results from the analysis of gasification, SOFC and PEME subsystems were compared with data from literature to validate model reliability. A comparison between the composition of dry syngas species from the gasification analysis of wood and those reported by Athari et al. [31] and Zainal et al. [39] are shown in Table 5A. The results show a deviation between 3 % and 9 % for the gas composition when compared with experimental data of Zainal et al. [39], except for CH<sub>4</sub>. This is attributed to the difference in the ultimate analysis of the combined biomass in this study and that of wood. The model validation for the SOFC is reported in Table 5B with cell voltage, V<sub>SOFC</sub>, and power density, ρ<sub>SOFC</sub>, compared with Holagh et al. [20]. The minimal error value of 0.6 %–2.4 % for V<sub>SOFC</sub> and 2.8 %–5.1 % for ρ<sub>SOFC</sub> show good agreement with the results of literature as they are within allowable range. The validity of the PEME data were compared to the study reported by Ref. [34], for the variation of electrolyzer voltage as presented in Table 5C.

The different thermodynamic properties at different points of the plant is shown in Table 6. This include the pressure, temperature, mass

**Table 5**  
Validation.

A. Gasification validation with wood at 1073 (K)						
Composition (%)	This study	Experiment data Zainal et al., 2001	Zainal et al., 2001	Athari et al., 2014		
N <sub>2</sub>	42.14	46.68	42.31	48.7		
H <sub>2</sub>	20.94	21.61	15.23	18.01		
CO <sub>2</sub>	13.04	12.01	16.42	13.84		
CO	21.01	19.61	23.04	18.77		
CH <sub>4</sub>	2.872	0.64	1.58	0.68		
O <sub>2</sub>	0	0	1.42	0		
Calorific value (MJ/m <sup>3</sup> )	5.029	4.72	4.85	–		
B. SOFC validation with related studies [20]						
j <sub>SOFC</sub> (A/m <sup>2</sup> )	V <sub>SOFC</sub> (V)			ρ <sub>SOFC</sub> (W/m <sup>2</sup> )		
	Present work	Ref.	Error (%)	Present work	Ref.	Error (%)
2000	0.779	0.790	1.4	0.163	0.158	3.2
3000	0.707	0.711	0.6	0.222	0.216	2.8
4000	0.636	0.644	1.2	0.266	0.253	5.1
5000	0.566	0.560	1.1	0.296	0.288	2.8
6000	0.498	0.510	2.4	0.312	0.301	3.7
C. PEME Validation [34]						
j <sub>E</sub> (A/m <sup>2</sup> )	V <sub>PEME</sub> (V)					
	Present work	Ref.	Error (%)			
6000	1.7	1.89	10.0			
8000	1.88	1.92	2.08			
10000	2.063	1.95	5.79			

**Table 6**

Thermodynamic properties for the stream of the proposed plant under base condition.

State	Fluid	P (kPa)	T (K)	$\dot{m}$ (kg/s)	Ex (kW)
1	Air	101.3	298.2	0.0277	0
2	Crop residue	101.3	298.2	0.0138	273.7
3	Syngas	101.3	1023	0.0415	213.9
4	Syngas	101.3	480	0.0415	178.6
4a	N <sub>2</sub>	101.3	330	0.0235	1.397
5	Syngas	101.3	330	0.0180	175.5
6	Animal waste + water	101.3	298.2	1.298	19938
7	CH <sub>4</sub> + CO <sub>2</sub>	101.3	328.2	1.208	17970
7a	CO <sub>2</sub>	101.3	300	0.8682	374.1
8	Water	101.3	327.6	0.0122	0.06829
9	Water	15.33	327.9	0.0122	0.1182
10	Steam	4000	561.9	0.0122	12.81
11	Steam	3880	561.9	0.0122	5.944
12	MM	3764	308.2	0.0496	0.0096
13	MM	9.374	308.8	0.0496	0.1251
14	MM	1745	429.9	0.0496	2.494
15	MM	1745	532	0.0496	8.899
16	MM	1745	459.2	0.0496	3.223
17	MM	9.374	312.8	0.0496	0.4168
18	Water	9.374	298.2	0.3288	0
19	Water	101.3	306.5	0.3288	0.1592
20	Water	101.3	343	0.0522	0.3014
21	Oxygen/Water	101.3	343	0.0495	12.21
22	Hydrogen	101.3	343	0.0023	278.7
23	Sludge	101.3	328.2	0.0907	1853
24	Syngas	101.3	345	0.0204	449.4
25	Syngas	101.3	500	0.0105	388.8
26	H <sub>2</sub> O	100	500	0.0099	5.643
27	CH <sub>4</sub>	100	298.2	0.3398	17594
28	CH <sub>4</sub>	101.3	554.9	0.3398	17785
29	CH <sub>4</sub>	1064	785.5	0.3398	17955
30	Off-gases	1042	1023	0.708	12411
31	Air	1022	298	10.58	0
32	Air	101.3	637.7	10.58	3370
33	Air	1064	785.5	10.58	4331
34	Air	1042	1023	10.17	6294
35	Exhaust gases	1022	1273	10.89	13612
36	Exhaust gases	1001	826.2	10.89	3612
37	Exhaust gases	108.2	811.5	10.89	3433
38	Exhaust gases	106	711.5	10.89	2415
39	Exhaust gases	103.9	528.3	10.89	903.9
40	Exhaust gases	101.8	506.5	10.89	738.9
41	Water	99.8	327.1	1.02	5.551
42	Water	15	327.6	1.02	11.83
43	Steam	6000	653.9	1.02	1229
44	Steam	6000	327.1	1.02	188.4
45	Water	15	298.2	83.03	0
46	Water	101.3	311.5	83.03	44.8
47	MM	101.3	308.2	1.019	0.1976
48	MM	9.374	308.8	1.019	2.568
49	MM	1745	419.1	1.019	43.87
50	MM	1745	522	1.019	170.3
51	MM	1745	446.5	1.019	57.76
52	MM	9.374	312.8	1.019	8.556
53	Water	9.374	298.2	19.64	0
54	Water	101.3	304.6	19.64	1.859

flow rate and exergy at each point in the plant. Each state point's reference condition is taken to be a temperature of 298.2 K and pressure of 101.3 kPa, respectively.

The analysis of the base case centered on the determination of the net power, efficiency and LCOE from the integration of the BCU and subsystems of the power plant. From Table 7, the overall energy and exergy performances of the proposed plant attained values of 44.93 % and 36.78 %, respectively. The net power was obtained as 7.42 MW, after a power consumption of 0.45 MW by the PEME. The LHV of syngas from gasification is upgraded from 4.20 MJ/kg to 37.79 MJ/kg with hydrogen from the PEME at flowrate of 0.0023 kg/s. ORC-I generates a net power of 4.98 kW, with thermal efficiency of 30.04 %. Also, in the base condition, the SOFC net power of 2.58 MW accounts for 34 % of the net power of the integrated plant and GT, ST and ORC-II net power

**Table 7**

Thermodynamic assessment results of the multigeneration power plant (base case).

Performance parameter	Value
LHV of biomass (MJ/kg)	17.697
Total mass flow rate of biomass (kg/s)	0.9821
Exergy of biomass (MJ/kg)	20.18
LHV syngas (MJ/kg)	4.20
LHV of biogas, CH <sub>4</sub> (MJ/kg)	15.22
LHV of upgraded syngas (MJ/kg)	37.79
ORC-I net power (kW)	4.95
PEME net voltage (V)	2.01
PEME power consumption (MW)	0.45
Mass flow rate of hydrogen for methanation	0.0121
Efficiency of PEME (%)	73.73
SOFC net voltage (V)	0.59
SOFC electrical power (MW)	2.58
Efficiency of SOFC (%)	40
GT net power (MW)	3.856
ST net power (MW)	0.89
Thermal efficiency of ST (%)	30.10
Exergy efficiency of ST (%)	36.81
ORC-II net power (MW)	0.098
Thermal efficiency of ORC-II (%)	30.07
Plant net power (MW)	7.42
Thermal efficiency of the plant (%)	44.93
Exergy efficiency of the plant (%)	36.78
LCOE (\$/MWh)	133.90

outputs were obtained as 3.856 MW, 0.89 MW and 0.098 MW, respectively. This is equivalent to subsystem power capacities of 20.64 GWh, 30.85 GWh, 7.12 GWh, 0.78 GWh and 0.03 GWh for the SOFC, GT, ST, ORC-II and ORC-I, respectively. Taking into account a per capita consumption of 135 kWh, the facility can therefore produce 59.42 GWh, or approximately one-fourth of the 240 GWh estimated as the locality's power demand. The levelized cost of electricity for the configuration is 133.9 \$/MWh. This is high when compared to average LCOE from bioenergy in selected regions by the international renewable energy agency, with cost of 58 \$/MWh for India, 60 \$/MWh for China, 88 \$/MWh for Europe and 77 \$/MWh for the rest of the world. However, it is within range of the LCOE of 250 \$/MWh for bioenergy electricity in areas with low-cost feedstocks [40].

### 3.3. Sensitivity analysis

In order to predict the plants response to changes in design parameters, a sensitivity analysis is presented in Figs. 2–9. This shows the net power, exergy efficiency and LCOE responses to the SOFC current density, SOFC-GT pressure ratio, combustion temperature, steam turbine inlet pressure, and six ORC working fluids in ORC I and II. The variation of the current density with net voltage, voltage loss and power density of the SOFC is presented in Fig. 2(a). The net voltage is significantly affected by current density, as it decreases with increasing current density. This is due to increasing voltage losses attributed to the combined effect of activation, ohmic and concentration losses in the SOFC. The power density of the SOFC increases significantly to a peak of 3.47 kW/cm<sup>2</sup> at 8000 A/m<sup>2</sup> before decreasing with increasing current density. This is as a result of material deterioration and high thermal losses associated with the SOFC at high current density values according to Karimi et al. [18]. Despite these effects on the SOFC, in Fig. 2(b), high current densities tend to enhance the plants  $\dot{W}_{Net}$  to an optimal value of 7.6 MW and minimum LCOE of 129 \$/MWh at  $j_{SOFC}$  of 8000 A/m<sup>2</sup>. This is proportional to the changes in the SOFC power output which has direct effect on  $\dot{W}_{Net}$  according to equation (33).

Fig. 3 shows that, as the compression pressure ratio  $r_p$  of the topping cycle increases,  $\dot{W}_{Net}$  and  $\eta_{ex}$  first increased to optimal values of 7.9 MW and 39.5 %, respectively, before decreasing. This can be attributed to an increment of the power generated by the GT compared to the power

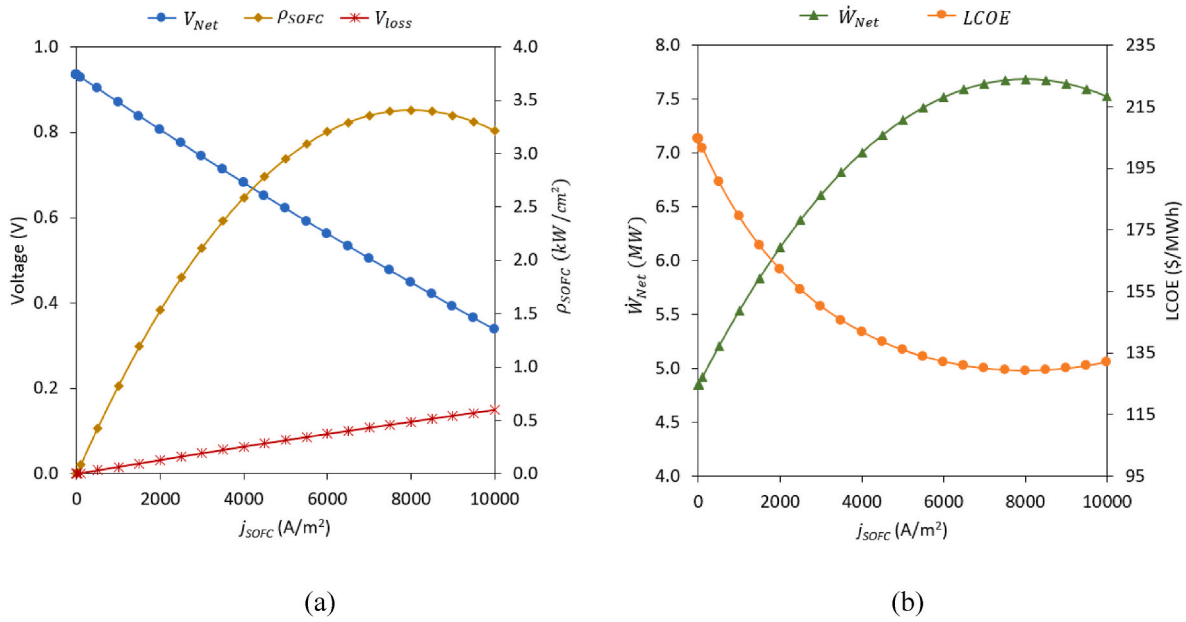


Fig. 2. Effect of SOFC current density,  $j_{SOFC}$  on net voltage, voltage loss, SOFC power density, net power and LCOE.

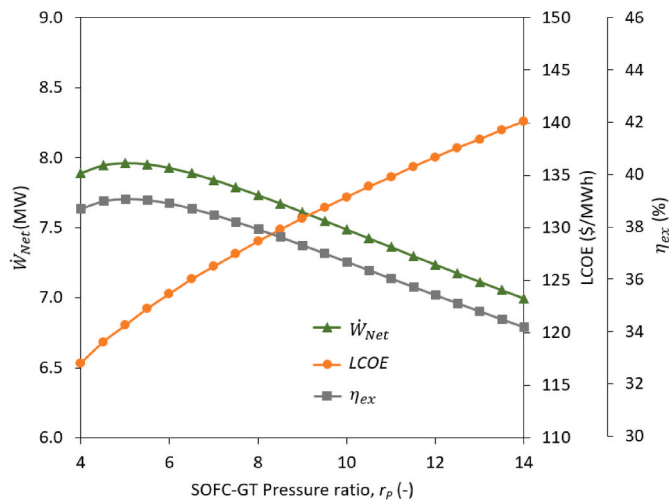


Fig. 3. Effect of topping cycle pressure ratio on plant performance.

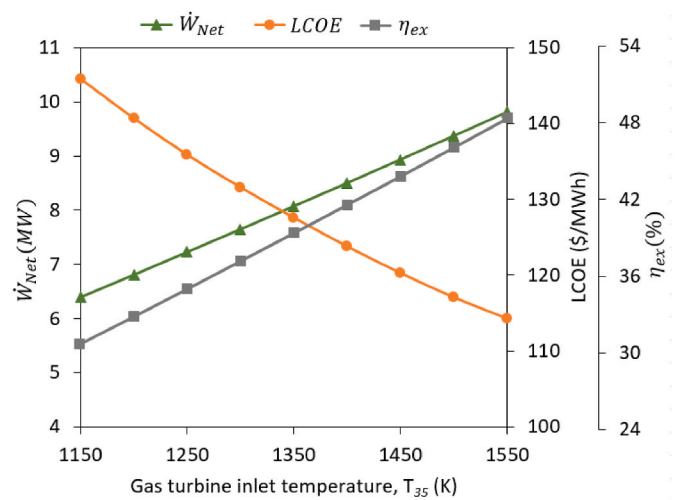


Fig. 4. Effect of turbine inlet temperature on system performance.

consumed by the compressors at low  $r_p$  values. The high compression ratio is undermined by the efficiency and requires high compression work [15]. Also, minimum LCOE occurred at minimum  $r_p$ , with corresponding high values of LCOE, low  $\dot{W}_{Net}$  and  $\eta_{ex}$  at high  $r_p$ . The effect of GT inlet temperature on the plant's performances is shown in Fig. 4. The net power,  $\dot{W}_{Net}$  and exergy efficiency,  $\eta_{ex}$  of the plant are improved by increasing the GT inlet temperature from 1150 K to 1550 K. This is due to the increase in enthalpy drop rate in the GT resulting in 36.8 % increase in its electrical power output. Hence the increase in the net power and exergy efficiency. Also, increase in the GT inlet temperature resulted in a decrease in LCOE, which is as a result of the increase in corresponding net power. However, there are limitations surrounding high turbine inlet temperatures due to the metallurgical properties of the turbine blades.

From Fig. 5(a) the steam turbine inlet pressure,  $P_{43}$ , is plotted against power output  $\dot{W}_{St,Net}$  and thermal efficiency  $\eta_{th,St}$  of the steam turbine unit. Increasing  $P_{43}$  yields corresponding decrease in  $\eta_{St,ex}$  up from 37.40 % to 32.29 %, however, a decreasing steam turbine power output from 0.90 MW to 0.78 MW is observed. This can be attributed to

the reduction in the specific volume of steam at high ST inlet pressures despite the increasing enthalpy change of the steam turbine. Whereas in Fig. 5(b), the net power of the plant increased by 0.5 % from 7.41 MW to 7.45 MW. The increase in the net power, is due to contributions from the other power cycles in the plant. However, an increase in the LCOE of the plant is observed and is as a result of the contributions of the ST unit to the LCOE of the plant. Low power outputs in the ST unit would yield high contributions to the plants LCOE.

The performance of ORC-I under six working fluids, with the effect on the net power of the integrated plant is presented in Fig. 6. With siloxane, MM, a net power and thermal efficiency of 4.62 kW and 28.02 %, and 5.34 kW and 32.39 % was obtained with MDM. The power output with organic fluids of cyclopentane and cyclohexane were obtained as 4.29 kW and 5.02 kW, with thermal efficiencies of 26.05 % and 30.46 %, respectively. From refrigerants, R1233zd(E) and R600a, power outputs of 3 kW and 2.35 kW, with efficiencies of 18.23 % and 14.28 %, respectively, were obtained. The siloxanes provided a higher power and efficiencies compared to the organic fluids and refrigerants. The variations in these results can be attributed to the different thermophysical

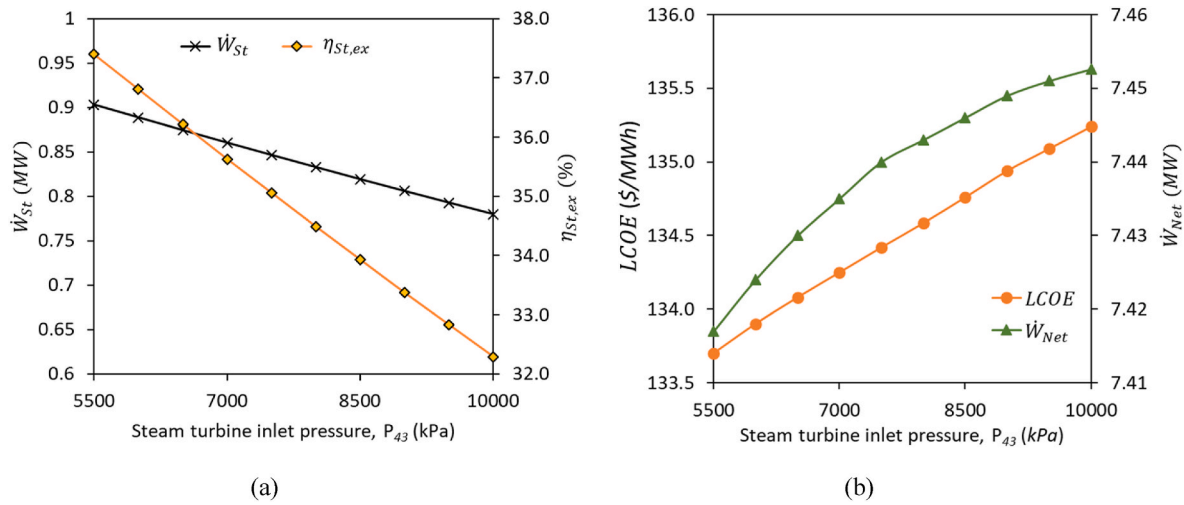


Fig. 5. Effect of steam turbine inlet pressure on net power and thermal efficiency of the steam turbine unit.

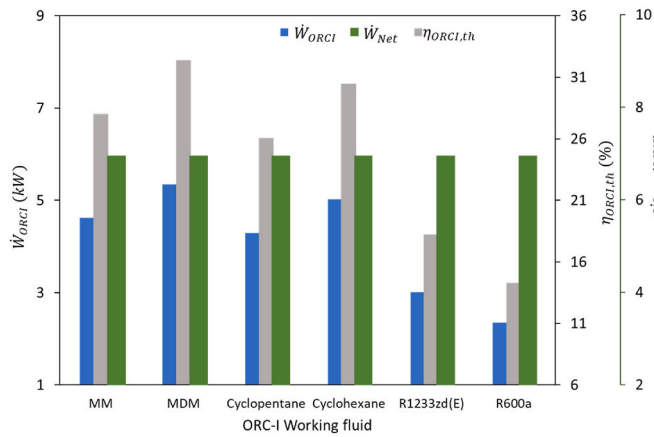


Fig. 6. Total power of combined plant with thermal efficiency and net power of ORC-I under different working fluids.

properties of these working fluids, as well as the amount of heat source for the ORC-I unit. However, the impact of the power output of ORC-I on the integrated plant shows no significant change on the net power of the plant.

The performance of the ORC-II under constant evaporator pressure, pinch point temperature and degree of superheat is shown in Fig. 7(a). MM and MDM as working fluid resulted in power outputs of 0.225 MW and 0.05 MW, respectively. The selected hydrocarbons, cyclopentane and cyclohexane resulted in ORC-II power outputs of 0.326 MW and 0.313 MW, respectively. Whereas, refrigerants R1233zd(E) and R600a resulted in power outputs of 0.206 MW and 0.273 MW, respectively. Subsequently, in Fig. 7(b), changes in the net power and LCOE of the integrated plant can be observed with the various working fluids. A net power of 7.38 MW and LCOE of 140  $\$/MWh$  was obtained for the integrated plant with MDM as working fluid in ORC-II. However, this improves to 7.55 MW with LCOE of 138  $\$/MWh$  using MM as working fluid. Cyclopentane provided power outputs of 7.65 MW, with LCOE of 136.7  $\$/MWh$ , and Cyclohexane produced 7.64 MW, and 136.9  $\$/MWh$ , respectively. With R1233zd(E) the plant's net power and LCOE were 7.53 MW and 138.5  $\$/MWh$ , and for R600a, 7.60 MW power output with LCOE of and 137.4  $\$/MWh$  was obtained. Despite high efficiencies recorded with the high temperature fluids of siloxanes, the hydrocarbons provided higher power output compared to the refrigerants and siloxanes. These variations indicate that the high evaporator pressure may not be suitable for all selected working fluids. Hence an optimization of the input parameters of the ORC-II is necessary to obtain optimum results.

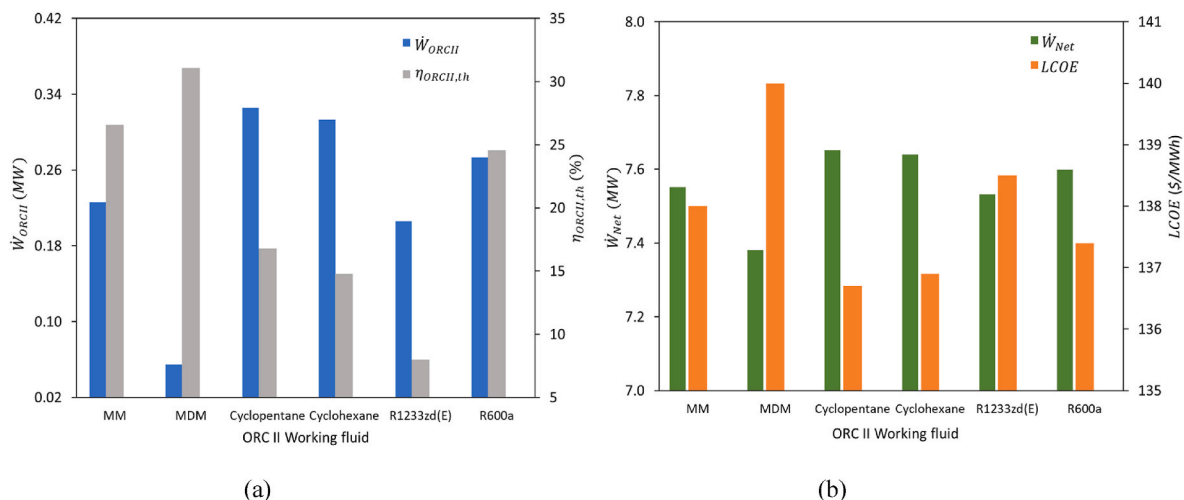
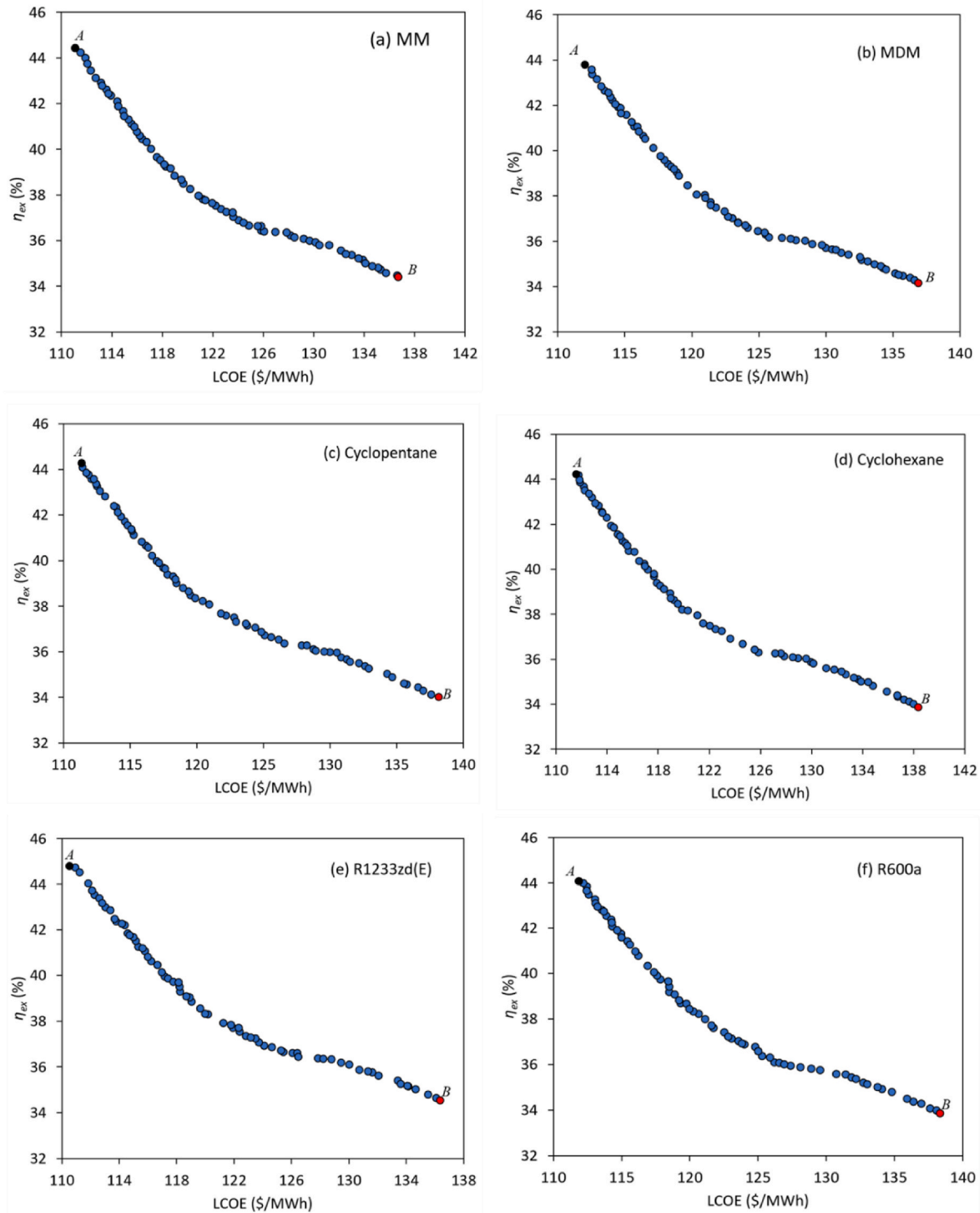


Fig. 7. ORC-II performance with net power and leveled cost of the plant.



**Fig. 8.** Pareto optimal solutions for power plant with ORC-II working fluids (a) MM (b) MDM (c) Cyclopentane (d) Cyclohexane (e) R1233zd(E) (f) R600a.

### 3.4. Optimization result

A MOGA optimization was used to optimize the power plant based on the sensitivity analysis. With the application of the optimization, a set of optimal values was generated and presented in a Pareto front curve with two objectives of minimizing the LCOE and maximizing the exergy efficiency as shown in Fig. 8. On the Pareto front curve, the two points A and B, identified on the top-left and bottom-right of the graph shows the maximum exergy efficiency and the minimum cost, respectively. These points also correspond to the optimal points for each single objective

function. Results shown in Table 8 indicate that the proposed plants exergy efficiency can be improved by 22 %, from 36.78 % to 44.93 %. This also attracts a reduction in LCOE from 133.9 \$/MWh base case to 111.8 \$/MWh and net power improvement from 7.42 to 9.05 MW, using R1233zd(E) in ORC-II. Low pressure ratio of 5.32–5.44 in the SOFC-GT unit provided high GT net power output of 4.777–4.828 MW. This shows agreement with Fig. 3 where maximum plant performance occurred within low pressure ratios of 4.5–5.5. Maximum current densities between 7222 and 7460 A/m<sup>2</sup> in the SOFC slightly increased the net power of the SOFC by a maximum of 2 %, due to the reduction in pressure ratio.

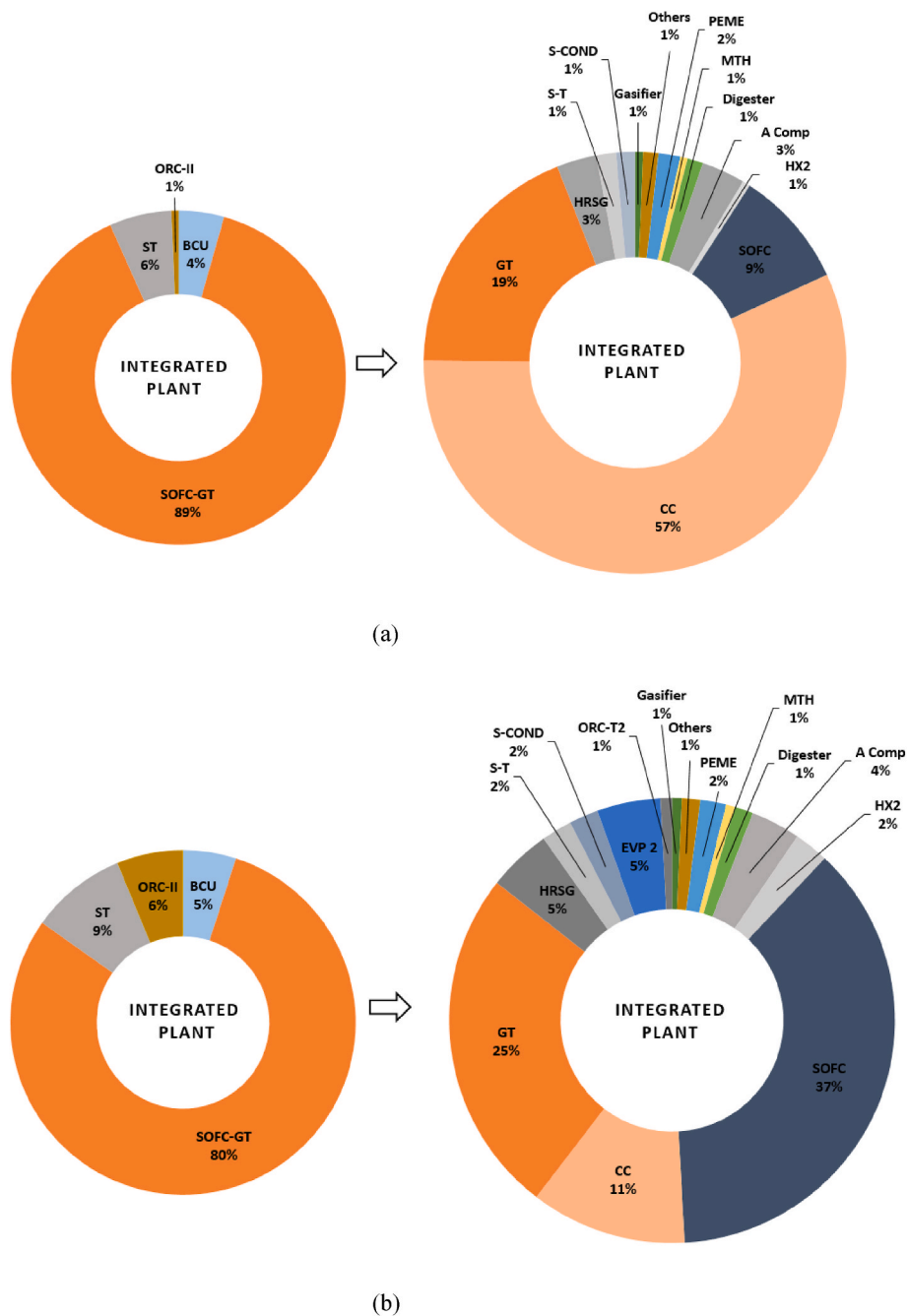


Fig. 9. Percentage distribution of exergy destruction across plant components of the integrated plant (a) before optimization (b) after optimization with R1233zd(E) in ORC-II.

High turbine inlet temperature of 1341 K, also contributed to the high-power output of the GT as optimum pressure ratios are enhanced with maximum temperatures. The net power of the ST was increased by 30.78 % from 0.89 kW to 1.164 MW at maximum pressure of 5838.81 kPa and pinch point of 16.72 K. The optimized results also indicated an increase in the net power of ORC-II from an initial 0.098 MW–0.431 MW with R600a. R1233zd(E) provided an output of 0.427 MW. With cyclopentane, cyclohexane, MM and MDM as working fluids, power outputs of 0.424 MW, 0.424 MW, 0.381 MW and 0.323 MW, were obtained, respectively. The high-power output of ORC-II with R600a as working fluid is due to the high-pressure factor and degree of superheat from the optimization analysis.

For the proposed system, the results of the exergy destruction on plant component basis is summarized in Fig. 9. The SOFC-GT unit has

the largest contribution to the total exergy destroyed with 89 % from which the combustion chamber (CC) accounts for 57 % in Fig. 9(a). In Fig. 9(b), which is obtained from Point A in Fig. 8(e), contribution from the SOFC-GT unit reduces to 80 %. The SOFC accounts for the largest contribution of 37 %, with CC reduced to 11 % and GT increased to 25 % after optimization. Both steam evaporator and heat recovery vapour evaporators increase to 5 %, respectively. These changes infer possible interaction of the parameters of the sub-systems in order to attain optimum performance.

The cost distribution of the subsystems on capital cost for the base case and optimized cases is shown in Fig. 10. The change between the base case and optimum cases is negligible for the BCU, SOFC-GT and ST, except in ORC-II. This signifies that likely increase in the integrated plants capital cost due to increase in plant capacity results in negligible

**Table 8**  
Decision variables and objective function values with different ORC-II working fluids at optimal point A.

Decision variables	Unit	Base case	ORCII Working fluid					
			MM	MDM	Cyclopentane	Cyclohexane	R1233zd(E)	R600a
$r_p$	—	10.5	5.43	5.32	5.44	5.42	5.32	5.38
$j_{SOFC}$	A/m <sup>2</sup>	5500	7460.26	7333.22	7334.58	7222.56	7244.20	7318.27
$T_{35}$	K	1273	1334.82	1331.94	1329.04	1333.35	1341.5	1329.52
$P_{43}$	kPa	6000	5312.77	6058.39	5979.17	6159.30	5838.81	6828.47
$\Delta p_{st}$	K	15	14.38	17.55	13.97	21.69	16.72	17.67
$\theta$	—	0.9	0.2532	0.2056	0.3041	0.2470	0.4156	0.6814
$\Delta p_{ORCII}$	K	10	5.14	7.78	6.35	6.02	5.04	5.43
$\Delta sh_{ORCII}$	K	10	4.33	4.98	4.75	5.64	6.54	7.23
<b>Objectives</b>								
$\dot{W}_{SOFC}$	MW	2.58	2.64	2.63	2.64	2.637	2.631	2.637
$\dot{W}_{GT}$	MW	3.856	4.789	4.777	4.746	4.782	4.828	4.756
$\dot{W}_{St}$	MW	0.89	1.17	1.12	1.13	1.097	1.164	1.086
$\dot{W}_{ORCII}$	MW	0.098	0.381	0.323	0.424	0.424	0.427	0.431
$\dot{W}_{Net}$	MW	7.42	8.98	8.85	8.94	8.94	9.05	8.91
$\eta_{th}$	%	44.93	54.36	53.58	54.16	54.11	54.81	53.93
$\eta_{ex}$	%	36.78	44.5	43.86	44.34	44.29	44.87	44.15
LCOE	\$/MWh	133.90	112.2	113.3	112.6	113.0	111.8	113.3

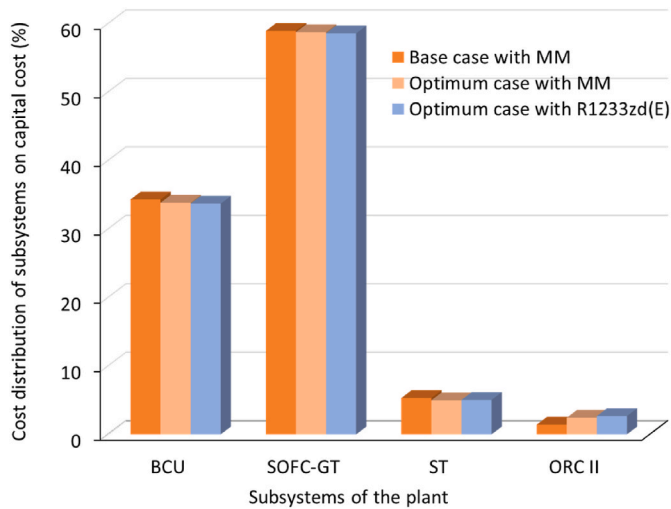


**Fig. 10.** Cost distribution of subsystems for base case and optimum cases with MM and R1233zd(E).

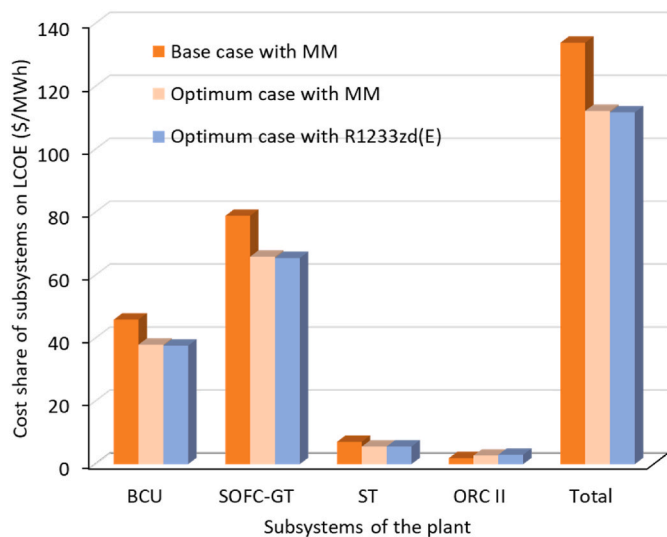


**Fig. 11.** Cost share of subsystems on LCOE under base case and optimum cases with MM and R1233zd(E).

cost effect in the subsystems. Fig. 11 presents the cost share of the different plant sections on LCOE for the base case and optimum cases with MM and R1233zd(E). The cost shares associated with the BCU, SOFC-GT and ST units are reduced after optimization with MM and R1233zd(E). However, in ORC-II, the cost share increased for the optimized cases. Hence, the gains of optimization can be seen in the reduction of total LCOE in Fig. 11, coupled with higher power outputs and exergy efficiency from the optimized cases as shown in Table 8.

Finally, the results of this study was compared with other studies with integrated subsystems in Table 9. The proposed configuration in this study exhibits maximum power and exergy efficiency of 9.05 MW and 44.87%, respectively, which is in competitive range of 4–16 MW and 42–59 % of the other studies with several outputs. From the comparison the integrated plant can achieve a balanced, positive energy source.

#### 4. Conclusion

In this study, an integrated bioconversion plant with a combined cycle power plant is proposed for power generation using biogas produced from digestion of animal waste and syngas from the gasification of crop waste. To enhance the energy content of the syngas, a methanation unit is introduced to convert the hydrogen produced from a PEME into upgraded synthetic gas. Fuel from the biomass conversion and upgrading processes is converted to power in a combined SOFC-GT topping cycle. The exhaust gas from the gas turbine is utilized in a ST and ORC unit for power generation. The plant is optimized in order to maximize the integrated plant's exergy efficiency while lowering LCOE by conducting a two-objective optimization. MOGA is applied in optimizing the plant utilizing EES and MATLAB. The desired working conditions are then determined by a trade-off between the optimized objectives using LINMAP decision-making method. The findings of this study can be summed up as follows:

- At optimum conditions, the net power generated by the SOFC, GT, ST and ORC-II is about 2.64 MW, 4.83 MW, 1.16 MW, and 0.427 MW, respectively. This, with power of ORC-I totals 9.05 MW as net power of the integrated plant.
- The LCOE is reduced to 111.8 \$/MWh from an initial 133.9 \$/MWh
- The overall energy and exergy efficiencies of the system at optimum points were obtained as 54.81 % and 44.87 %, respectively.
- The components with the most contribution to exergy destruction are SOFC (37 %), CC (11 %), GT (25 %) after optimization.
- Performance of refrigerants (R1233zd(E) and R600a) as working fluid in ORC-II is better than siloxanes (MM and MDM), and

**Table 9**  
Comparison of results of biomass conversion systems with this study.

Study	Year	Subsystems	Results
Balafkandeh et al. [29]	2019	Biomass gasifier, digester, GT, S-CO <sub>2</sub> , Absorption refrigeration	Net exergy efficiency 47.8 % and Unit cost of product of 5.436 \$/GJ.
Yilmaz et al. [27]	2019	Biomass gasifier, GT, Kalina cycle, reverse osmosis unit, PEME, Absorption cooling cycle, dryer and heat pump.	Total power of 15 MW with hydrogen production of 0.072 kg/s Energy and exergy efficiencies of 63.84% and 59.26%, respectively. Cooling effect of 4.36 MW. Heating effect of 5 MW Cost rate of 2000 \$/s Net power of 4.4 MW, with 71 % contribution from SOFC. Cooling effect of 0.16 MW. 0.00155 kg/s rate of hydrogen and, 0.96 kg/s of freshwater. Overall energy and exergy efficiencies of 77.6% and 47.1%, respectively. Cost per unit exergy of 11.28 \$/GJ.
Holagh et al. [20]	2020	CH <sub>4</sub> fueled SOFC, GT, with biomass combustor, ORC, PEME and desalination unit	Net Power of 16.5 MW. Exergy efficiency of 56.69 %. Specific cost of 5.65 \$/GJ.
Al-Rashed and Afrand [28]	2021	Biomass, Anaerobic digester, GT, S-CO <sub>2</sub> , Absorption refrigeration	Net Power of 8.9 MW. Energy and exergy efficiencies of 71.13 % and 42.03 %, respectively. Heat load of 4.24 MW Specific cost of 10.94 \$/GJ.
He et al. [6]	2022	Biomass gasifier, GT, Stirling engine, S-CO <sub>2</sub> cycle and domestic water heater	Net Power of 9.05 MW and SOFC contribution of 29 %. Hydrogen flow rate of 0.0023 kg/s. LHV of upgraded syngas of 37.78 MJ/kg Energy and exergy efficiencies of 54.81 % and 44.87 %, respectively. Levelized cost of electricity of 111.8 \$/h
This study	2023	Biomass, Anaerobic digester, Gasifier, PEME, Syngas upgrade, SOFC, GT, ST and ORC	

hydrocarbons (cyclopentane and cyclohexane) with refrigerant

**Appendix A**

Energy and exergy balance equations of the integrated plant components.

Component	Energy balance equation	Exergy balance equations
Gasifier	$\dot{m}_3 h_3 = \dot{m}_1 h_1 + \dot{m}_2 h_2$	$\dot{E}_{X_{D,G}} = \dot{E}_{X_1} + \dot{E}_{X_2} - \dot{E}_{X_3}$
P1	$\dot{W}_{P1} = \dot{m}_8 (h_9 - h_8)$	$\dot{E}_{X_{D,P1}} = \dot{W}_{P1} + \dot{E}_{X_8} - \dot{E}_{X_9}$
HXS	$\dot{m}_3 (h_3 - h_4) = \dot{m}_9 (h_{10} - h_9)$	$\dot{E}_{X_{D,HXS}} = \dot{E}_{X_3} - \dot{E}_{X_4} + \dot{E}_{X_{10}} - \dot{E}_{X_9}$
SC	$\dot{m}_4 h_4 = \dot{m}_{4a} h_{4a} + \dot{m}_5 h_5$	$\dot{E}_{X_{D,SC}} = \dot{E}_{X_4} - \dot{E}_{X_{4a}} - \dot{E}_{X_5}$
ORC P1	$\dot{W}_{ORC,P1} = \dot{m}_8 (h_{13} - h_{12})$	$\dot{E}_{X_{D,ORC,P1}} = \dot{W}_{ORC,P1} + \dot{E}_{X_{12}} - \dot{E}_{X_{13}}$
REG	$\dot{m}_{16} (h_{16} - h_{17}) = \dot{m}_{13} (h_{14} - h_{13})$	$\dot{E}_{X_{D,REG}} = \dot{E}_{X_{13}} - \dot{E}_{X_{14}} + \dot{E}_{X_{16}} - \dot{E}_{X_{17}}$
EVP	$\dot{m}_{10} (h_{10} - h_{11}) = \dot{m}_{14} (h_{15} - h_{14})$	$\dot{E}_{X_{D,EVP}} = \dot{E}_{X_{10}} - \dot{E}_{X_{11}} + \dot{E}_{X_{14}} - \dot{E}_{X_{15}}$
ORC T	$\dot{W}_{T1} = \dot{m}_{15} (h_{15} - h_{16})$	$\dot{E}_{X_{D,ORC,T}} = \dot{E}_{X_{15}} - \dot{E}_{X_{16}} - \dot{W}_{T1}$
COND	$\dot{m}_{17} (h_{17} - h_{12}) = \dot{m}_{18} (h_{19} - h_{18})$	$\dot{E}_{X_{D,COND1}} = \dot{E}_{X_{17}} - \dot{E}_{X_{12}} + \dot{E}_{X_{18}} - \dot{E}_{X_{19}}$
PEME	$\dot{W}_{PEME} + \dot{m}_{20} h_{20} = \dot{m}_{21} h_{21} + \dot{m}_{22} h_{22}$	$\dot{E}_{X_{D,PEME}} = \dot{W}_{PEME} + \dot{E}_{X_{20}} - \dot{E}_{X_{21}} - \dot{E}_{X_{22}}$

(continued on next page)

R600a reaching net power of 0.427 MW. However, the R1233zd(E) is selected as working fluid based on the integrated plant's net power and LCOE.

- In ORC-I, maximum power output of 4.985 kW is obtained with MDM with as working fluid.
- Hydrogen produced at 0.0028 kg/s with power input of 0.45 MW from the SOFC, was used in upgrading the syngas via a methanation process.

Thus, the integration of the syngas upgrade to the biomass-to-energy plant further strengthens the utilization of integrated plants in attaining sustainable energy goals. For future studies, the steam supplied to ORC-I can be utilized for other purposes such as steam refrigeration or process heat. Also, an exergo-economic analysis and environmental impact should also be considered.

**CRedit authorship contribution statement**

**O.J. Ogorure:** Conceptualization, Data curation, Formal analysis, Funding acquisition, Methodology, Validation, Writing – original draft. **F. Heberle:** Project administration, Supervision, Validation, Visualization, Writing – review & editing. **D. Brüggemann:** Funding acquisition, Project administration, Supervision, Validation, Visualization, Writing – review & editing.

**Declaration of competing interest**

The authors declare that they have no known competing financial interests or personal relationships that could have appeared to influence the work reported in this paper.

**Acknowledgement**

The authors acknowledge the sponsorship of this work by the Petroleum Technology Development Fund (PTDF)/Deutscher Akademischer Austauschdienst (DAAD) partnership under the Nigerian-German Postgraduate Training Programme 2019 (57473408).

(continued)

Component	Energy balance equation	Exergy balance equations
Valve	$\dot{m}_5 h_5 + \dot{m}_{22} h_{22} = \dot{m}_{24} h_{24}$	$\dot{E}X_{D,Valve} = \dot{E}X_{22} + \dot{E}X_5 - \dot{E}X_{24}$
MTH	$\dot{m}_{24} h_{24} = \dot{m}_{25} h_{25} + \dot{m}_{26} h_{26}$	$\dot{E}X_{D,MTH} = \dot{E}X_{24} - \dot{E}X_{25} - \dot{E}X_{26}$
Digester	$\dot{m}_6 h_6 = \dot{m}_7 h_7 + \dot{m}_{23} h_{23}$	$\dot{E}X_{D,AD} = \dot{E}X_6 - \dot{E}X_7 - \dot{E}X_{23}$
BC	$\dot{m}_7 h_7 = \dot{m}_{7a} h_{7a} + \dot{m}_{27} h_{27}$	$\dot{E}X_{D,BC} = \dot{E}X_7 - \dot{E}X_{7a} - \dot{E}X_{27}$
F-COMP	$\dot{W}_{F,k} = \dot{m}_{27} (h_{28} - h_{27})$	$\dot{E}X_{D,F,k} = \dot{W}_{F,k} + \dot{E}X_{27} - \dot{E}X_{28}$
HX1	$\dot{m}_{28} (h_{29} - h_{28}) = \dot{m}_{36} (h_{36} - h_{37})$	$\dot{E}X_{D,HX1} = \dot{E}X_{28} - \dot{E}X_{29} + \dot{E}X_{36} - \dot{E}X_{37}$
A-COMP	$\dot{W}_{A,k} = \dot{m}_{31} (h_{31} - h_{32})$	$\dot{E}X_{D,A,k} = \dot{W}_{A,k} + \dot{E}X_{31} - \dot{E}X_{32}$
HX2	$\dot{m}_{32} (h_{33} - h_{32}) = \dot{m}_{37} (h_{37} - h_{38})$	$\dot{E}X_{D,HX2} = \dot{E}X_{32} - \dot{E}X_{33} + \dot{E}X_{37} - \dot{E}X_{38}$
SOFC	$\dot{m}_{29} h_{29} + \dot{m}_{33} h_{33} = \dot{m}_{30} h_{30} + \dot{m}_{34} h_{34} + \dot{W}_{SOFC}$	$\dot{E}X_{D,SOFC} = \dot{E}X_{29} - \dot{E}X_{30} + \dot{E}X_{33} - \dot{E}X_{34} - \dot{W}_{SOFC}$
CC	$\dot{m}_{30} h_{30} + \dot{m}_{34} h_{34} + \dot{m}_{25} h_{25} = \dot{m}_{35} h_{35}$	$\dot{E}X_{D,CC} = \dot{E}X_{30} + \dot{E}X_{34} + \dot{E}X_{25} - \dot{E}X_{35}$
GT	$\dot{W}_{Gt} = \dot{m}_{35} (h_{35} - h_{36})$	$\dot{E}X_{D,Gt} = \dot{E}X_{35} - \dot{E}X_{36} - \dot{W}_{Gt}$
HRSG	$\dot{m}_{38} (h_{38} - h_{39}) = \dot{m}_{42} (h_{43} - h_{42})$	$\dot{E}X_{D,HRSG} = \dot{E}X_{38} - \dot{E}X_{39} + \dot{E}X_{42} - \dot{E}X_{43}$
S-P	$\dot{W}_{SP} = \dot{m}_{41} (h_{42} - h_{41})$	$\dot{E}X_{D,S,P} = \dot{W}_{S,P} + \dot{E}X_{41} - \dot{E}X_{42}$
S-T	$\dot{W}_{St} = \dot{m}_{43} (h_{44} - h_{43})$	$\dot{E}X_{D,St} = \dot{E}X_{43} - \dot{E}X_{44} - \dot{W}_{St}$
S-COND	$\dot{m}_{42} (h_{44} - h_{42}) = \dot{m}_{45} (h_{46} - h_{45})$	$\dot{E}X_{D,S-COND} = \dot{E}X_{44} - \dot{E}X_{41} + \dot{E}X_{45} - \dot{E}X_{46}$
ORC-P2	$\dot{W}_{ORC,P2} = \dot{m}_{47} (h_{48} - h_{47})$	$\dot{E}X_{D,ORC,P2} = \dot{W}_{ORC,P2} + \dot{E}X_{47} - \dot{E}X_{48}$
EVP 2	$\dot{m}_{39} (h_{39} - h_{40}) = \dot{m}_{49} (h_{50} - h_{49})$	$\dot{E}X_{D,EVP2} = \dot{E}X_{39} - \dot{E}X_{40} + \dot{E}X_{49} - \dot{E}X_{50}$
REG 2	$\dot{m}_{48} (h_{49} - h_{48}) = \dot{m}_{51} (h_{51} - h_{52})$	$\dot{E}X_{D,REG2} = \dot{E}X_{48} - \dot{E}X_{49} + \dot{E}X_{51} - \dot{E}X_{52}$
ORC-T2	$\dot{W}_{ORC,T2} = \dot{m}_{50} (h_{50} - h_{51})$	$\dot{E}X_{D,ORC,T2} = \dot{E}X_{50} - \dot{E}X_{51} - \dot{W}_{T2}$
ORC COND	$\dot{m}_{47} (h_{52} - h_{47}) = \dot{m}_{53} (h_{54} - h_{53})$	$\dot{E}X_{D,COND2} = \dot{E}X_{52} - \dot{E}X_{47} + \dot{E}X_{53} - \dot{E}X_{54}$

## Appendix B

Parameters in plant component cost estimation [15,20,37,38].

	$K_1$	$K_2$	$K_3$	$B_1$	$B_2$	$C_1$	$C_2$	$C_3$	$f_M$	$f_{BM}$
Pump	3.3892	0.0536	0.1538	1.89	1.35	-0.3935	0.3957	-0.00226	1.55	-
ORC-T	2.6259	1.4398	-0.1776							3.5
HRVG	4.8306	-0.8509	0.3187	1.63	1.66	0.03881	-0.011272	0.08183	1.8	
Regenerator	2.7652	-0.7282	0.0783	1.74	1.55				1.25	1.25
Condenser	4.8306	-0.8509	0.3187	1.63	1.66	0.03881	-0.011272	0.08183	1.8	
MTH	4.1052	0.5320	-0.0005	L = 5[m], D = 0.95[m]						4
Compressor	2.2898	1.3604	-0.1027							2.8
HX fuel	3.3444	-0.2745	-0.0472	1.74	1.55				1.25	1.25
HX Air	3.3444	-0.2745	-0.0472	1.74	1.55				1.25	1.25
Gas Turbine	-21.77	13.2175	-1.5279							3.5
HRSG	4.8306	-0.8509	0.3187	1.63	1.66	0.03881	-0.011272	0.08183	1.8	
ST	2.6259	1.4398	-0.1776							3.5
CC	$48.64 \dot{m}_{34} (1 + \exp(0.018T_{35} - 26.4)) (0.995 - \frac{P_{35}}{P_{34}})^{-1} Z_f$									
Gasifier	$1600(3600 \dot{m}_{biomass})^{0.67} Z_f$									
Digester	$350000 (\frac{\dot{v}_r}{21000 m^3})^{0.75} Z_f$									
SOFC	$A_{act} N_{FC} (2.96 T_{SOFC} - 1907) Z_f$									
Inverter	$100000 (\frac{\dot{W}_{SOFC}}{500})^{0.7} Z_f$									
PEME	$1000 \dot{W}_{PEME} Z_f$									

CEPCI<sub>2020</sub> = 596.2.

CEPCI<sub>2011</sub> = 397 [37].

## References

- [1] F. Safari, I. Dincer, Development and analysis of a novel biomass-based integrated system for multigeneration with hydrogen production, *Int. J. Hydrogen Energy* 44 (2019) 3511–3526, <https://doi.org/10.1016/j.ijhydene.2018.12.101>.
- [2] N.V. Emodi, K.J. Boo, Sustainable energy development in Nigeria: Overcoming energy poverty, *Int. J. Energy Econ. Pol.* 5 (2015) 580–597.
- [3] K. Owebor, E.O. Diemuodeke, T.A. Briggs, M. Imran, Power Situation and renewable energy potentials in Nigeria – a case for integrated multi-generation technology, *Renew. Energy* 177 (2021) 773–796, <https://doi.org/10.1016/j.renene.2021.06.017>.
- [4] NREEEP, National renewable energy and energy efficiency policy (Nreeep), 2015, *Jikken Dobutsu* 31 (2015) 323–325.
- [5] F.O. Olanrewaju, G.E. Andrews, H. Li, H.N. Phylaktou, Bioenergy potential in Nigeria, *Chem Eng Trans* 74 (2019) 61–66, <https://doi.org/10.3303/CET1974011>.
- [6] F. He, X. Liu, M. Wang, S. Zhou, D. Heydarian, Energy, exergy, exergoeconomic, and environmental analyses and multi-objective optimization of a biomass-to-energy integrated thermal power plant, *Alex. Eng. J.* 61 (2022) 5629–5648, <https://doi.org/10.1016/j.aej.2021.11.016>.
- [7] F. Monlau, M. Francavilla, C. Sambusiti, N. Antoniou, A. Solhy, A. Libutti, A. Zabaniotou, A. Barakat, M. Monteleone, Toward a functional integration of anaerobic digestion and pyrolysis for a sustainable resource management. Comparison between solid-digestate and its derived pyrochar as soil amendment, *Appl. Energy* 169 (2016) 652–662, <https://doi.org/10.1016/j.apenergy.2016.02.084>.
- [8] A. Wellinger, J. Murphy, D. Baxter, *The Biogas Handbook: Science, Production and Applications*, 2013, <https://doi.org/10.1533/9780857097415>.
- [9] G. Lozza, Syngas Cooling in IGCC Systems, Elsevier Ltd, 2017, <https://doi.org/10.1016/B978-0-08-100167-7.00009-3>.
- [10] A. Molino, G. Braccio, Synthetic natural gas SNG production from biomass gasification - thermodynamics and processing aspects, *Fuel* 139 (2015) 425–429, <https://doi.org/10.1016/j.fuel.2014.09.005>.
- [11] X. He, A novel hybrid digestion-gasification process integrated with membranes for efficient conversion of biomass to bio-alcohols, *Green Energy Environ.* 6 (2021) 15–21, <https://doi.org/10.1016/j.gee.2020.04.003>.

- [12] O.J. Ogorure, F. Heberle, D. Brüggemann, Thermodynamic analysis of a combined organic Rankine cycle (ORC) with proton exchange membrane electrolyzer (PEME) in an integrated biomass conversion system, in: ORC2021, 6th Int. Seminar on ORC Power Systems, Munich, 2021, pp. 1–9, <https://doi.org/10.14459/2021mp1632937>.
- [13] K. Mohammadi, J.G. McGowan, K. Powell, Thermoeconomic analysis of a multigeneration system using waste heat from a triple power cycle, Appl. Therm. Eng. 190 (2021) 1–30, <https://doi.org/10.1016/j.applthermaleng.2021.116790>.
- [14] Z. Wang, Energy and Air Pollution 1–5 (2018), <https://doi.org/10.1016/B978-0-12-809597-3.00127-9>.
- [15] O.J. Ogorure, C.O.C. Oko, E.O. Diemuodeke, K. Owebor, Energy, exergy, environmental and economic analysis of an agricultural waste-to-energy integrated multigeneration thermal power plant, Energy Convers. Manag. 171 (2018) 222–240, <https://doi.org/10.1016/j.enconman.2018.05.093>.
- [16] N. Tukenmez, M. Koc, M. Ozturk, A novel combined biomass and solar energy conversion-based multigeneration system with hydrogen and ammonia generation, Int. J. Hydrogen Energy 46 (2021) 16319–16343, <https://doi.org/10.1016/j.ijhydene.2021.02.215>.
- [17] M.H. Taheri, A.H. Mosaffa, L.G. Farshi, Energy, exergy and economic assessments of a novel integrated biomass based multigeneration energy system with hydrogen production and LNG regasification cycle, Energy 125 (2017) 162–177, <https://doi.org/10.1016/j.energy.2017.02.124>.
- [18] M.H. Karimi, N. Chitgar, M.A. Emadi, P. Ahmadi, M.A. Rosen, Performance assessment and optimization of a biomass-based solid oxide fuel cell and micro gas turbine system integrated with an organic Rankine cycle, Int. J. Hydrogen Energy 45 (2020) 6262–6277, <https://doi.org/10.1016/j.ijhydene.2019.12.143>.
- [19] E. Soleymani, S. Ghavami Gargari, H. Ghaebi, Thermodynamic and thermoeconomic analysis of a novel power and hydrogen cogeneration cycle based on solid SOFC, Renew. Energy 177 (2021) 495–518, <https://doi.org/10.1016/j.renene.2021.05.103>.
- [20] S.G. Holagh, M.A. Haghghi, Z. Mohammadi, A. Chitsaz, Exergoeconomic and environmental investigation of an innovative poly-generation plant driven by a solid oxide fuel cell for production of electricity, cooling, desalinated water, and hydrogen, Int. J. Energy Res. 44 (2020) 10126–10154, <https://doi.org/10.1002/er.5626>.
- [21] M.A. Emadi, N. Chitgar, O.A. Oyewunmi, C.N. Markides, Working-fluid selection and thermoeconomic optimisation of a combined cycle cogeneration dual-loop organic Rankine cycle (ORC) system for solid oxide fuel cell (SOFC) waste-heat recovery, Appl. Energy 261 (2020) 114384, <https://doi.org/10.1016/j.apenergy.2019.114384>.
- [22] E. Sevinchan, I. Dincer, H. Lang, Energy and exergy analyses of a biogas driven multigenerational system, Energy (2018), <https://doi.org/10.1016/j.energy.2018.10.085>.
- [23] M. Malik, I. Dincer, M.A. Rosen, Development and analysis of a new renewable energy-based multi-generation system, Energy 79 (2015) 90–99, <https://doi.org/10.1016/j.energy.2014.10.057>.
- [24] P. Ahmadi, I. Dincer, M.A. Rosen, Development and assessment of an integrated biomass-based multi-generation energy system, Energy 56 (2013) 155–166, <https://doi.org/10.1016/j.energy.2013.04.024>.
- [25] O. Bamisile, Q. Huang, M. Dagbasi, M. Taiwo, V. Adebayo, Energy, exergy and environmental analyses of a biomass driven multi-generation system, Int. J. Energy 31 (2020) 249–267, <https://doi.org/10.1504/IJEX.2020.106454>.
- [26] S. Anvari, H. Taghavifar, A. Parvishi, Thermo-economic consideration of Regenerative organic Rankine cycle coupling with the absorption chiller systems incorporated in the trigeneration system, Energy Convers. Manag. 148 (2017) 317–329, <https://doi.org/10.1016/j.enconman.2017.05.077>.
- [27] F. Yilmaz, M. Ozturk, R. Selbas, Development and techno-economic assessment of a new biomass-assisted integrated plant for multigeneration, Energy Convers. Manag. 202 (2019) 112154, <https://doi.org/10.1016/j.enconman.2019.112154>.
- [28] A.A.A. Al-Rashed, M. Afrand, Multi-criteria exergoeconomic optimization for a combined gas turbine-supercritical CO<sub>2</sub> plant with compressor intake cooling fueled by biogas from anaerobic digestion, Energy 223 (2021) 119997, <https://doi.org/10.1016/j.energy.2021.119997>.
- [29] S. Balafkandeh, V. Zare, E. Gholamian, Multi-objective optimization of a tri-generation system based on biomass gasification/digestion combined with S-CO<sub>2</sub> cycle and absorption chiller, Energy Convers. Manag. 200 (2019) 112057, <https://doi.org/10.1016/j.enconman.2019.112057>.
- [30] S. Georgousopoulos, K. Braimakis, D. Grimekis, S. Karellas, Thermodynamic and techno-economic assessment of pure and zeotropic fluid ORCs for waste heat recovery in a biomass IGCC plant, Appl. Therm. Eng. 183 (2021) 116202, <https://doi.org/10.1016/j.applthermaleng.2020.116202>.
- [31] H. Athari, S. Soltani, S.M. Seyed Mahmoudi, M.A. Rosen, T. Morosuk, Exergoeconomic analysis of a biomass post-firing combined-cycle power plant, Energy (2014), <https://doi.org/10.1016/j.energy.2014.09.033>.
- [32] G. Allesina, S. Pedrazzi, L. Guidetti, P. Tartarini, Modeling of coupling gasification and anaerobic digestion processes for maize bioenergy conversion, Biomass Bioenergy 81 (2015) 444–451, <https://doi.org/10.1016/j.biombioe.2015.07.010>.
- [33] J. Gao, Y. Wang, Y. Ping, D. Hu, G. Xu, F. Gu, F. Su, A thermodynamic analysis of methanation reactions of carbon oxides for the production of synthetic natural gas, RSC Adv. 2 (2012) 2358–2368, <https://doi.org/10.1039/c2ra00632d>.
- [34] E.W. Saeed, E.G. Warkozek, Modeling and analysis of renewable PEME fuel cell system, Energy Proc. 74 (2015) 87–101, <https://doi.org/10.1016/j.egypro.2015.07.527>.
- [35] S.L. Douvartzides, A. Tsiolikas, N.D. Charisiou, M. Souliotis, V. Karayannis, N. Taousanidis, Energy and exergy-based screening of various refrigerants, hydrocarbons and siloxanes for the optimization of biomass boiler–organic rankine cycle (BB–ORC) heat and power cogeneration plants, Energies 15 (2022), <https://doi.org/10.3390/en15155513>.
- [36] D. Buentello-Montoya, X. Zhang, An energy and exergy analysis of biomass gasification integrated with a char-catalytic tar reforming system, Energy Fuel. 33 (2019) 8746–8757, <https://doi.org/10.1021/acs.energyfuels.9b01808>.
- [37] R. Turton, R.C. Bailie, W.B. Whiting, J.A. Shaeiwitz, D. Bhattacharyya, Analysis, Synthesis, and Design of Chemical Processes, fourth ed., Prentice Hall, Upper Saddle River, NJ (USA), 2012. ISBN 0975442201.
- [38] J.G. Andreasen, E. Baldasso, M.R. Kærn, T. Weith, F. Heberle, D. Brüggemann, F. Haglind, Techno-economic feasibility analysis of zeotropic mixtures and pure fluids for organic Rankine cycle systems, Appl. Therm. Eng. 192 (2021) 116791, <https://doi.org/10.1016/j.applthermaleng.2021.116791>.
- [39] Z.A. Zainal, R. Ali, C.H. Lean, K.N. Seetharamu, Prediction of performance of a downdraft gasifier using equilibrium modeling for different biomass materials, Energy Convers. Manag. 42 (2001) 1499–1515, [https://doi.org/10.1016/S0196-8904\(00\)00078-9](https://doi.org/10.1016/S0196-8904(00)00078-9).
- [40] International Renewable Energy Agency, Renewable Power Generation Costs in 2020, 2020. Abu Dhabi. ISBN 978-92-9260-348-9.
- [41] H. Sayyaadi, Modeling, Assessment, and Optimization of Energy Systems, Elsevier, 2021. ISBN 978-0-12-816656-7.

## Nomenclature

### Symbols

- A: Activation area, (m<sup>2</sup>)  
 Ex: Exergy rate, (kW)  
 e: Specific exergy, (kW/kg)  
 F: Faraday constant, (C/mol)  
 G: Gibbs free energy, (kJ)  
 g: Specific Gibbs free energy, (kJ/kmol)  
 h: Specific enthalpy, (kJ/kg)  
 I: Current, (A)  
 j: Current density, (A/m<sup>2</sup>)  
 K: Equilibrium constant  
 ṁ: mass flow rate, (kg/s)  
 N: Number of cells  
 ṅ: molar flow rate, (kmol/s)  
 P: Pressure, (kPa)  
 Q̇: Rate of heat transfer, (kW)  
 s: specific entropy, (kJ/kgK)  
 r: Pressure ratio  
 T: Temperature, (K)  
 V: Voltage, (V)  
 Ẇ: Power, (kW)  
 Z: Cost rate

### Subscript and superscripts

- 0: Ambient condition  
 a: Anode  
 act: activation  
 ca: cathode  
 ch: chemical  
 conc: concentration  
 cr: critical  
 E: electrolyzer  
 eff: effective  
 ex: exergy  
 FC: fuel cell  
 Net: net value  
 ph: physical  
 ohm: Ohmic  
 orc: organic Rankine cycle  
 PEM: proton exchange membrane  
 sofc: solid oxide fuel cell  
 st: steam turbine  
 th: thermal

### Greek symbols

- α: number of electrons  
 β: exergy ratio  
 η: efficiency, (%)  
 ρ: power density, (kW/cm<sup>2</sup>)  
 σ: PEME conductivity  
 λ: water content at anode and cathode  
 μ: Chemical potential  
 θ: pressure factor of ORC